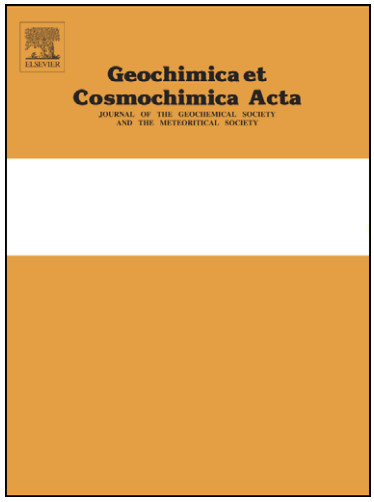

Ab initio molecular dynamics simulation and free energy exploration of copper (I) complexation by chloride and bisulfide in hydrothermal fluids

Yuan Mei, David M. Sherman, Weihua Liu, Joël Brugger

PII: S0016-7037(12)00609-6
DOI: http://dx.doi.org/10.1016/j.gca.2012.10.027
Reference: GCA 7972

To appear in: *Geochimica et Cosmochimica Acta*

Received Date: 3 April 2012
Accepted Date: 15 October 2012

Please cite this article as: Mei, Y., Sherman, D.M., Liu, W., Brugger, J., *Ab initio* molecular dynamics simulation and free energy exploration of copper (I) complexation by chloride and bisulfide in hydrothermal fluids, *Geochimica et Cosmochimica Acta* (2012), doi: http://dx.doi.org/10.1016/j.gca.2012.10.027

Ab initio molecular dynamics simulation and free energy exploration of copper (I) complexation by chloride and bisulfide in hydrothermal fluids

Yuan Mei[1, 2, 3], David M Sherman[2], Weihua Liu[3] and Joël Brugger[1,4,*]

[1] School of Earth and Environmental Sciences, The University of Adelaide, Adelaide, SA 5005, Australia

[2] Department of Earth Sciences, University of Bristol, Bristol, BS8 1RJ, UK

[3] CSIRO Earth Science and Resource Engineering, Clayton, VIC 3168, Australia

[4] South Australian Museum, North Terrace, SA 5000, Australia

* Corresponding author, joel.brugger@adelaide.edu.au

Abstract

Chloride and bisulfide are the primary ligands believed to control the transport of copper in hydrothermal fluids. *Ab initio* molecular dynamics (MD) simulations based on density functional theory were conducted to predict the stoichiometries and geometries of Cu(I) complexes in mixed chloride and hydrosulfide (HS^- and H_2S(aq)) fluids at ambient temperature and at 327 ˚C and 500 bar, and to assess the relative importance of the chloride and hydrosulfide ligands for Cu transport. The simulations accurately reproduce the identity and geometries of Cu(I) chloride and bisulfide species derived from experimental solubility, UV-Vis, and *in situ* XAS results. The simulations indicate the following ligand preference: $HS^- > Cl^- > H_2S$ for Cu(I) complexes, but predict a high stability of the mixed-ligand complex, $CuCl(HS)^-$, a species that has never been investigated experimentally. The thermodynamic properties (formation constants, logKs) of Cu(I) chloride and bisulfide complexes were investigated by distance-constrained MD simulations using thermodynamic integration. The predicted logKs of the following reactions are in good agreement (within 1 log unit) with the experimental values (Brugger et al., 2007; Liu W et al., 2001):

$$Cu^+ + Cl^- = CuCl\,(aq);\ \log K_{327^\circ C,calc} = +3.87 \pm 0.14;\ \log K_{325^\circ C,exp} = +4.12;$$

$$CuCl(aq) + Cl^- = CuCl_2^-;\ \log K_{327^\circ C,calc} = +2.84 \pm 0.09;\ \log K_{325^\circ C,exp} = +1.98;$$

$$CuCl_2^- + Cl^- = CuCl_3^{2-};\ \log K_{327^\circ C,calc} = -1.23 \pm 0.21;\ \log K_{325^\circ C,exp} = -2.17.$$

The fair agreements between the predicted logKs with those derived from experimental data demonstrates the potential of predicting thermodynamic properties for transition metal complexes under hydrothermal conditions by MD simulations. The formation constant for the mixed-ligand complex $CuCl(HS)^-$ is calculated for the first time:

$$Cu^+ + Cl^- + HS^- = CuCl(HS)^-;\ \log K_{327^\circ C,calc} = +11.47.$$

Determination of the formation constants for Cu(I) complexes enabled the construction of activity-activity diagrams entirely based on the MD simulation data. The results suggest that the mixed-ligand complex plays an important role in Cu transport in hydrothermal fluids.

Keywords: Copper, bisulfide complexes, chloride complexes, hydrothermal ore deposits, *ab initio* molecular dynamic simulations, thermodynamic properties.

1 Introduction

1.1 Molecular understanding of metal transport in hydrothermal fluids

Understanding the speciation of metals in hydrothermal fluids underpins our ability to predict element mobility in natural and man-made systems (e.g., formation of ore deposits; hydrometallurgy; corrosion in power plants; Seward and Driesner, 2004). For example, hydrothermal ore deposits contain most of the Au, Ag, U, Fe, Mn, Zn, Pb or Mo resources within the Earth's crust. Consequently, understanding the mechanisms of metal transport and deposition in hydrothermal systems under wide ranges of fluid composition, pressure and temperature is essential for the development of mineral exploration technologies and to maintain the rate of discovery of new deposits. Metals are transported as aqueous metal complexes in ore-forming fluids (Seward and Barnes, 1997). Over the past 15 years, experimental and theoretical advances have transformed our understanding of hydrothermal ore transport and deposition. The availability of third-generation synchrotron sources, linked with the development of spectroscopic autoclaves, enables routine measurements of high-quality X-ray absorption spectroscopy (XAS) data on aqueous solutions beyond the critical point of water. Using such techniques, a large amount of data about the molecular-level speciation of metals in fluids at elevated P-T have been generated (e.g., Brugger et al., 2010; Seward and Driesner 2004). At the same time, molecular dynamics (MD) simulations allow us to explore metal speciation and, as will be shown here, even derive thermodynamic properties. Such simulations can be an important adjunct to spectroscopic measurements of speciation and can explore PT regimes not accessible via experiment. Several groups have combined MD and EXAFS spectroscopy to study the stoichiometry and geometry of aqueous metal complexes (e.g., D'Angelo et al., 2002; 2006; Dang et al., 2006; Fulton et al., 2009; Hoffmann et al., 1999).

In this study, we use *ab initio* (i.e., first principles) MD simulations to study the stoichiometry and geometry of Cu(I) complexes in chloride- and hydrosulfide-brines at 27 ˚C and 327 ˚C. This chemical system was chosen not only because of its relevance in the formation of copper deposits, but also because of the large amount of high quality experimental data obtained over the past decade by a number of methods and research groups on the nature and geometry of Cu(I) complexes under hydrothermal conditions. These data enable us to test the accuracy of the predictions of the MD simulations. We then explore the

predictive capabilities of MD simulations and their ability to discover new complexes and predict thermodynamic properties for important complex-forming reactions.

1.2 Experimental studies of Cu-Cl and Cu-HS/H_2S complexes

Copper can form various complexes with the valence states of +1 and +2 in natural waters, and *in situ* measurements of natural fluid inclusions and synthetic solutions show that Cu(I) is the predominant oxidation state under hydrothermal conditions (Brugger et al., 2007; Mavrogenes et al., 2002). The hydrosulfide (mainly HS^- and possibly $H_2S(aq)$) and chloride (Cl^-) ligands are particularly important for the transport of copper in hydrothermal fluids (e.g., Etschmann et al., 2010). A large number of solubility, *in situ* ultra-violet-visible (UV-Vis) spectroscopy, and XAS studies have been conducted to investigate Cu(I) speciation and retrieve thermodynamic properties for the important complexes from ambient to supercritical conditions (Archibald et al., 2002; Brugger et al., 2007; Crerar and Barnes, 1976; Etschmann et al., 2010; Fritz, 1980, 1981; Fulton et al., 2000a, 2000b; Hemley et al., 1992; Liu W et al., 2001, 2002; Mountain and Seward, 1999, 2003; Seyfried Jr and Ding, 1993; Var'yash, 1992; Xiao et al., 1998). For Cu(I) bisulfide complexes, the current consensus is that Cu(HS)(aq) and $Cu(HS)_2^-$ are the predominant species, with $Cu(HS)_2^-$ becoming more important with increasing temperature (Etschmann et al., 2010). For chloride complexes, the suggested predominant species include CuCl(aq), $CuCl_2^-$ and $CuCl_3^-$ (Brugger et al., 2007).

To interpret the experimental data correctly, it is essential to choose the correct speciation model. For most solubility and UV-Vis studies under hydrothermal conditions, the speciation model is generated on the basis of the knowledge of low-T speciation and general considerations of the chemistry of the system. This can lead to wrong models and thus incorrect conclusions (see discussions in Brugger et al., 2007 and Sherman, 2007). *In situ* XAS data enable characterization of the molecular structures and stoichiometry of metal complexes over a wide range of temperatures and pressures, thus providing an independent confirmation of the speciation model that can help cross check and interpret solubility and UV-Vis data. In particular, knowledge of the geometry of the complexes places strong constraints on the range of possible species (e.g., discussion in Etschmann et al., 2011). XAS was employed to study Cu-Cl and Cu-HS/H_2S complexing under hydrothermal conditions (Brugger et al., 2007; Etschmann et al., 2010; Fulton et al., 2000a). These studies demonstrated that linear Cu(I) complexes (e.g., $[H_2O\text{-}Cu\text{-}Cl](aq)$; $[Cl\text{-}Cu\text{-}Cl]^-$; $[HS\text{-}Cu\text{-}SH]^-$) dominate Cu(I) speciation in chloride and hydrosulfide brines. The distorted trigonal species

$[CuCl_3]^{2-}$ plays a minor role in chloride-rich brines at low temperature (<200 ˚C; Brugger et al., 2007). These XAS data discredited the tetrahedral species $[CuCl_4]^{3-}$, a species postulated on the ground of its stability in coordination compounds, and led to a re-interpretation of earlier UV-Vis data (e.g., Liu W et al., 2002), and greatly improved our understanding of the speciation and thermodynamic properties of Cu transport in hydrothermal fluids.

The role of H_2S^0 as a ligand competing with HS^- and Cl^- is also a controversial topic. Based on XAS measurements, Pokrovski et al. (2009) suggested that the H_2S^0 ligand may contribute to the increasing solubility of gold in acidic fluids via formation of the $Au(HS)(H_2S)^0$ complex. This result was confirmed by the *ab initio* MD simulations of Liu X et al. (2011b). Crerar and Barnes (1976) interpreted their chalcopyrite solubility studies in terms of $Cu(HS)_2^-$ and $Cu(HS)_2(H_2S)^-$ as the predominant species under hydrothermal conditions (200-350 ˚C), indicating that H_2S^0 is a potential ligand for forming complexes with Cu(I). In more recent studies of Cu(I) hydrosulfide speciation, however, $Cu(HS)_2^-$ was interpreted as the stable complex by solubility measurements (Mountain and Seward, 1999, 2003) and by the XAS study of Etschmann et al. (2010). Note that $Cu(HS)(H_2S)^0$ could not be excluded on the basis of the XAS data, and that this species may be important in the vapor phase (Etschmann et al., 2010).

1.3 Molecular dynamics simulations of metal complexes in hydrothermal geochemistry

Classical MD simulations where atomic interactions are described using empirical interatomic potentials have been successfully employed to investigate aqueous solutions of alkali and alkaline earth metals at different T-P conditions (Dang et al., 2006; Driesner et al., 1998; Harris et al., 2001; John P, 1998; Sherman and Collings, 2002; Sherman, 2010). Such simulations accurately predict fluids density, cluster structures, pair distributions and phase diagrams. However, simple pair potentials fail to give a reliable description of the interatomic interactions involving transition metals like Cu, Ni, or Au (Hoffmann et al., 1999; Sherman, 2010). For such systems, the interatomic interactions need to be described quantum mechanically. *Ab initio* MD simulations solve the classical equations of motion but treat the interatomic interactions quantum mechanically using density functional theory (Car and Parrinello, 1985). In an early application to hydrothermal fluids, Harris et al. (2003) determined Zn(II) speciation in chloride-rich brines from room temperature to hydrothermal conditions using Born-Oppenheimer *ab initio* MD simulations, and were able to reproduce accurately the stoichiometry and geometry of Zn(II) chlorocomplexes at 25 ˚C and 300 ˚C up

to high salt concentrations of 7.4 m (reviews in Liu W et al., 2007; 2012). The implementation of *ab initio* molecular dynamics using the Car-Parrinello method (Car and Parrinello, 1985) enables simulations to be done on larger systems for longer times. Using this method, Sherman (2007) explored the speciation of Cu(I) chloro-complexes. In this study, it was found that Cu(I) exists as $CuCl_3^{2-}$ in a 4 m chloride solution at room temperature, with the third Cl^- ligand being only weakly bound; at high temperature, the linear $CuCl_2^-$ complex predominates, even with excess chloride in the solution. This study also concluded that the tetrahedral $CuCl_4^{3-}$ complex proposed for example by the UV-Vis study of Liu W et al. (2002) is not stable in aqueous solution; this theoretical prediction was independently confirmed by the XAS study of Brugger et al. (2007). Similar good agreement between calculated and measured speciation and complex geometries were obtained by Liu X et al. (2011b, 2012) in their *ab initio* MD simulations of the Au(I) hydrosulfide- and Ag(I) chloride-complexes. Therefore, *ab initio* MD simulations show good potential for predicting the aqueous speciation of transition metals.

The determination of thermodynamic properties for aqueous complexes, however, is a more significant challenge for MD simulations. Two techniques, metadynamics and thermodynamic integration, enable us to predict the free energy surface of complex-formation reactions (Sherman, 2010). Metadynamics (Alessandro and Francesco, 2008; Laio and Parrinello, 2002) is a powerful algorithm that can be used both for reconstructing the free energy of complexes and for accelerating rare events, eliminating the need to conduct long simulations. Once the reaction path and free energy profiles have been qualitatively explored by metadynamics, thermodynamic integration (Sprik, 1998) could be employed to calculate the free energy of predefined reaction coordinates. Van Sijl et al. (2010) employed metadynamics to explore the free energy surface of Ti(IV) in water at 300 K and 1000 K by constraining the Ti-O coordination number, and found that a 5-fold Ti(IV) aqua complex was stable at room temperature and a six-fold aqua complex at 1000 K. The Ag(I) MD studies of Liu X et al. (2012) qualitatively explored the free energy surface of Ag-Cl ligand dissociation reactions at 300 K by metadynamics and predicted the weak stability of trigonal planar $AgCl_3^{2-}$ under hydrothermal conditions. The hydration mechanisms of Zn^{2+} (Liu X et al., 2011a), Al^{3+} (Liu X et al., 2010b) and Cu^{2+} (Liu X et al., 2010a) have been investigated by coordination number constrained thermodynamic integration, and the predicted stabilities of hydration cations and hydration numbers show good agreement with experiments. Bühl and coworkers (Bühl and Golubnychiy, 2007; Bühl et al., 2006, 2008) constrained the bond distances of uranium-chloride and uranium-oxygen to predict the stoichiometry and free

energies for the formation of aqua- and chloride complexes of U(VI) at ambient conditions. The computations revealed significant solvent effects on geometric and energetic parameters, and confirmed the low affinity of uranyl for chloride in aqueous solutions. Those studies of free energy exploration illustrate the potential of predicting thermodynamic properties by MD simulation. In hydrothermal geochemistry, the estimation of thermodynamic properties via MD simulations would be especially useful due to the increasing difficulty of experimental measurements with increasing T and P.

1.4 Aims

Despite the number of studies that have been conducted on the Cu(I) chloride and hydrosulfide systems, there is still a lack of unambiguous identification of the predominant copper species in bisulfide and in particular mixed chloride-bisulfide solutions, which is more appropriate for natural hydrothermal systems than solutions containing only chloride or hydrosulfide. XAS is unable to reliably distinguish O and S atom around copper atoms (Etschmann et al., 2010), whereas *ab initio* MD simulations can provide insight into this problem. As experimental studies of Cu(I) chloride/bisulfide complexation have well characterized many important Cu(I) complex-forming reactions, this system is well suited for testing the ability of distance-constrained MD to produce accurate thermodynamic properties for important complex-forming reactions. Assessing the ability of the thermodynamic integration method in MD simulation to predict the thermodynamic properties of metal complexes under hydrothermal conditions is highly desirable, since this technique may ultimately be able to predict metal speciation and mobility in hydrothermal fluids beyond experimental conditions.

The specific aims of this study are to 1) predict the nature and geometry of the predominant Cu(I) species in bisulfide, chloride, and mixed chloride-bisulfide hydrothermal fluids using *ab initio* MD; in particular, assess the potential of mixed-ligand complexes to contribute to Cu(I) transport in hydrothermal fluids; and 2) predict thermodynamic properties (stability constants) for the important Cu(I) complexes using distance-constrained thermodynamic integration, and assess the suitability of the method for the study of hydrothermal solutions.

2 Computational methods

2.1 Car-Parrinello Molecular Dynamics Simulations

In this study, we used the Car-Parrinello (CP) molecular dynamics code CPMD (Car and Parrinello, 1985) to investigate the nature and geometry of copper (I) complexes in chloride and hydrosulfide hydrothermal fluids. Car-Parrinello *ab initio* molecular dynamics simulations implement density functional theory using a plane-wave basis set and pseudo-potentials for the core electrons. The PBE exchange correlation-functional (Perdew et al., 1996) was employed with a cutoff of gradient correction 5×10^{-5}. Lin et al. (2012) showed that the energy profiles for liquid water calculated by PBE agree very well with higher-level ab initio calculations (MP2, CCSD). Plane-wave cutoffs of 25 Ry (340.14 eV) were used together with Vanderbilt ultrasoft pseudo-potentials in CPMD package generated using the valence electron configuration $3d^{9.5}4s^{1}4p^{0.5}$ (Laasonen et al., 1993). Molecular dynamics simulations were conducted in the NVT ensemble (Sherman, 2007). A time-step of 3 a.u. (0.073 fs) was used to stabilize the simulations. Temperatures were controlled by the Nose thermostat for both the ions and electrons. Fictitious electron masses of 400 a.u. (3.644×10^{-28} kg) and target fictitious kinetic energies of 0.02 a.u. (52.49 kJ·mol^{-1}) were used to obtain convergence of the energy of the total CP-Hamiltonians. Periodic boundary conditions were used to eliminate surface effects. Classical MD was used to generate initial atomic configurations using the SPC/E potential for water (Berendsen et al., 1987; Smith and Dang, 1994) and approximate pair potentials derived from finite cluster calculations for Cu-Cl, Cu-S and Cu-O (Guymon et al., 2008, see Table A1 for details).

To investigate the stability of Cu complexes with different ligands, we calculated six different systems with different hydrosulfide/chloride ratios and concentrations. The compositions and box sizes of the simulated systems are shown in Table 1. Compared to classical MD, *ab initio* MD needs larger computing resources, so simulation boxes with ~180 atoms were chosen to provide manageable computation times while enabling the simulation of realistic solution compositions. The volumes of the simulation boxes were chosen in order for the densities to correspond to the equation of state of NaCl fluids at the same ionic strength at the pressure and temperature of interest (Driesner, 2007; Driesner and Heinrich, 2007). Stable Cu(I) complexes formed within 0 to 2 picoseconds (ps) of simulation time, depending on the simulated system and initial configuration. To achieve good statistics for the radial distribution functions (RDF), all the simulations were calculated for more than 10 ps

(1.38×10^5 steps). The simulation with excess chloride (No. 4) was run for ~ 20 ps to observe Cl-Cl ion exchange reactions.

2.2 *Ab initio* thermodynamic integration and free energy calculations

The free energies of the ion-exchange reactions are crucial for investigating the equilibrium formation constants of the $CuCl_x^{1-x}$ and $Cu(HS)_x^{1-x}$ complexes. We used the thermodynamic integration method (Resat, 1993; Sprik, 1998) to calculate the free energy surfaces for the formation reactions of these complexes at both ambient and hydrothermal conditions. The Cu(I)-ligand distances were constrained along predefined reaction paths, and the mean constraint force *f(r)* was obtained as a function of constrained distances by sampling possible configurations of Cu(I) complexes and the surrounding solvent and ions at each distance-constraint.

For example, the free energy of a ligand exchange reaction such as

$$[Cl\text{-}Cu\text{-}Cl]^- + H_2O = [H_2O\text{-}Cu\text{-}Cl]_{(aq)} + Cl^- \quad (1),$$

can be calculated by integrating the time-averaged constraint force, f(r) with respect to the constrained distance, r (Sprik, 1998; Bühl et al., 2006; 2008):

$$\Delta A_{a\to b} = -\int_a^b \langle f(r)\rangle dr \quad (2).$$

Here, f(r) is the force necessary to maintain the second chloride ion at a distance r from the Cu(I) ion, where r varies from 'infinity' (i.e., no interaction with the Cu(I) complex) to a bonded state. The thermodynamic integration runs were started by first equilibrating the initial configuration. Then, a series of constrained *ab initio* MD simulations were performed along the reaction coordinate defined by fixing the bond distances of the Cu-Cl or Cu-S pairs, until the final target configuration was obtained. Other simulation parameters were kept identical in the constrained and unconstrained simulations. All the constrained simulations were calculated for more than 3.6 ps, including 0.7 ps for equilibration (Bühl et al., 2006; 2008). Figure 1 shows the constraint force f(r) and its running average for the Cu-Cl pair at the distance of 4.25 Å at 327 ˚C. The running average of the constraint force converged in 1 (e.g., Fig. 1) to 3 ps. The average of the constraint force along the whole simulation was employed as the mean force for each configuration.

Figure 2 shows two examples of the reaction coordinates (reaction paths) from configuration **i** to **ii** and the constrained distances. As shown in Figure 2(a), for the reaction (1) in the initial configuration **i (reactants)**, one Cl was constrained at the distance of 2.12 Å,

corresponding to the equilibrium bonding distance. The other two free Cl^- ions were constrained at longer distances (6.00 Å), corresponding to distances at which atomic interactions between Cu and Cl are close to zero; this constraint was necessary to prevent the free Cl^- ions from complexing to Cu(I) when one Cl^- moved away. The other bonding Cl^- ion was allowed to move freely, and remained bonded to Cu(I) at a distance around 2.15 Å. When moving the Cl^- ion away from Cu(I), one water came close and bonded to Cu. In configuration **ii (products)**, the Cl^- ion on the reaction path was moved from 2.12 Å to 5 Å and replaced by an H_2O molecule, the two free Cl^- ions were still fixed at 6.00 Å. The unconstrained Cl^- and an unconstrained oxygen (H_2O) bonded to Cu(I) to form the linear $CuCl(H_2O)_{(aq)}$ complex.

To test the stability of $CuCl_3^{2-}$ at 327 ˚C, the free energy of the association reaction

$$CuCl_2^- + Cl^- = CuCl_3^{2-} \quad (3)$$

was calculated. As shown in Figure 2(b), in this case, both of the bonding Cl^- ions were constrained at 2.21 Å (the equilibrated bond length of $CuCl_3^{2-}$) in configuration **i (reactants)**. For the remaining two chloride ions, one was constrained at a long distance (6.00 Å) and the other at the reaction coordinates (from 5 Å to 2.38 Å). This was necessary to avoid losing one of the two bonded Cl^- ligands upon moving the third Cl^- towards the Cu(I) (i.e., effectively exchanging two chloride ions in $CuCl_2^-$), since $CuCl_2^-$ is the predominant complex at 327 ˚C.

As the calculations were conducted at constant volume, the retrieved free energies (equation (2)) correspond to the Helmholtz free energy. To compare with literature values of the thermodynamic properties of copper complexes, we need to calculate the Gibbs free energies at constant pressure. However, in *ab initio* MD, it is difficult to perform free energy calculations in the isobaric-isothermal ensemble (Haile, 1992). Therefore, it is practical to calculate the Gibbs free energies of the reactions from Helmholtz free energies by adding the energy changes due to the change of pressure,

$$\Delta G^r = \Delta A_{a\to b} + V\int_{p_0}^{p} dp, \quad (4)$$

where $\int_{p_0}^{p} dp$ is the accumulation of pressure change. The magnitude of the difference between ΔA and ΔG was estimated by considering the changes in apparent partial molar volumes of reactants and products during the reaction on the basis of molar volumes for individual aqueous species reported by Brugger et al. (2007) and Sverjensky et al. (1997) (see Table A2 for details). The energy difference for the ligand exchange reactions is in the order of 10-100 J mol^{-1} (i.e., ≤0.01 on the logK). This contribution is much smaller than the error

obtained by experiments or MD thermodynamic integration, so the Gibbs free energies of the reaction were approximated by the Helmholtz free energy, i.e., $\Delta_r G = \Delta A_{a \to b}$. This approximation has been adopted before by a number of authors (e.g., Habershon and Manolopoulos, 2011; Bühl et al., 2006; 2008; 2011; Mangold et al., 2011).

2.3 Correction of standard state and calculation of formation constants

The standard state Gibbs free energy of reaction $\Delta_r G^{\ominus}$ (the hypothetical 1 m concentrations with properties of infinite dilution) can be calculated from the Gibbs free energy of the reaction ($\Delta_r G$) obtained from thermodynamic integration, according to

$$\Delta_r G^{\Theta} = \Delta_r G + RT \ln \frac{C_A \gamma_A \cdot C_B \gamma_B}{C_C \gamma_C \cdot C_D \gamma_D} \qquad (5)$$

where C_i are the concentrations of reactants or products of the reaction A + B → C + D, and γ_i are the corresponding activity coefficients. For calculating $\Delta_r G^{\ominus,c}$ we assume unit activity coefficients. Since the metal and ligands exist at high concentrations (1-4 molal) in the simulated systems, and hence the solutions are far from the standard state, we also used the B-dot extension of the Debye-Hückel theory to estimate activity coefficients for the individual ions (Mambote et al., 2003; Zeng et al., 2008).

$$\log \gamma_i = -\frac{z_i^2 A_\gamma I^{1/2}}{1 + \mathring{a}_i B_\gamma I^{1/2}} + \dot{B}_\gamma I \qquad (6)$$

where z_i is the charge of ion, I is the ionic strength in the molality scale (m), $\mathring{a}_i$ is the ion size parameter in angstrom ($\mathring{a}_i$ = 5 for copper ions and complexes, $\mathring{a}_i$ = 4 for chloride ions). A_γ and B_γ are defined in Table 1 and Table 2 in Helgeson (1969). $\dot{B}_\gamma$ is an empirical parameter defined in Table 26 in Helgeson and Kirkham (1974). After activity corrections, the standard Gibbs free energy changes for each reaction, $\Delta_r G^{\Theta}$, were obtained. Then the formation constants were calculated from:

$$\Delta_r G^{\ominus} = - RT \ln K^{\ominus} \qquad (7)$$

3 Results

3.1 *Ab initio* molecular dynamic simulations

The results of *ab initio* molecular dynamics simulations are compiled in Table 1, and the Cu-Cl and Cu-S distances as a function of simulation time at 327 ˚C (~500 bar) are shown in Figure 3. The distribution functions showing the coordination numbers and distances are plotted in Figures 4 and 5 for the Cu-Cl and Cu-S pairs, respectively.

In simulation No.1, with a Cl concentration of 4 molal and sulfur existing only as $H_2S_{(aq)}$, Cu(I) existed as the $CuCl_2^-$ complex over the whole 14 ps of the simulation (Figure 3(a)). The vibrations of the Cu-Cl bonds in the $CuCl_2^-$ complex shown in Figure 3(a) correspond to vibration frequencies of $8.6*10^{12}$ Hz (287 cm^{-1}) and $11.6*10^{12}$ Hz (387 cm^{-1}); these values are close to those calculated for a gas-phase $CuCl_2^-$ cluster (280 and 373 cm^{-1}; Sherman 2007). The oscillations of the Cu-Cl bond length specify a Debye-Waller factor of 0.00638 $Å^2$, within error of that refined from the experimental EXAFS data by Brugger et al. (2007) (0.007(1) $Å^2$). The distribution function of Cu-Cl pairs shown in Figure 4(a) indicates that the Cu-Cl bond length is ~2.13 Å. The pair distribution function of Cu-S is very noisy (Figure 5(a)), and there is no obvious association between Cu and H_2S. The Cu-Cl bond lengths (2.13 Å) are in excellent agreement with those measured experimentally (2.152(7) Å, Brugger et al., 2007; 2.12-2.13 Å, Fulton et al., 2000a, 2000b). Furthermore, it is noteworthy that the simulated average Cl-Cu-Cl bond angle of 164(10)˚ is within error of the value of 161.5˚ derived from EXAFS data (Brugger et al., 2007), thus both the MD simulations and EXAFS experimental data confirm a distorted linear structure for the $CuCl_2^-$ complex. This simulation also indicates that the presence of H_2S(aq) does not change Cu speciation or the geometry of the $CuCl_2^-$ complex (e.g., chloride complexes predominate in acidic, S-rich brines).

In simulations 2 and 3 (Table 1), the H_2S molecules were replaced by HS^- and Na^+. This leads to the formation of a previously unknown $CuCl(HS)^-$ complex (Figure 3(b)). Interestingly, the expected $Cu(HS)_2^-$ complex does not form in simulation 3 at 327 ˚C, suggesting that the mixed-ligands complex is dominant in this fluid (see discussion below). The radial distribution functions for the Cu-Cl (Figure 4(b, c)) and Cu-S pairs (Figure 5(b, c)) confirm that the number of Cl^- and HS^- around Cu^+ is one for each, and Cu-Cl and Cu-S bond lengths are ~2.16 Å and ~2.15 Å, respectively.

To test the stability of the $CuCl(HS)^-$ complex in solutions with high Cl^- but low HS^- concentrations, a simulation was conducted for Cu^+ in 10 m Cl^- and 1 m HS^- (simulation No. 4). With the presence of excess chloride, $CuCl(HS)^-$ still predominates in the system, with minor amounts of the $[CuCl_2(HS)]^{2-}$ species, where the additional chloride is weakly bonded (Figure 3(c)). The $[CuCl_2(HS)]^{2-}$ species is also seen in Figure 3(c) to serve as a short-lived intermediary species in the exchange of two Cl^- ions. The Cu-Cl pair distribution function (Figure 4(d)) shows that the average number of Cl within 3 Å is ~1.2. We tentatively conclude that the $CuCl(HS)^-$ complex may be an important species in ore-forming solutions. We note that it would be difficult to distinguish between $CuCl(HS)^-$, $CuCl_2^-$ and $Cu(HS)_2^-$ using XAS (Etschmann et al. 2010).

In the Cl-free solution with 2 molal HS^- (simulation No. 5), Cu(I) forms a $Cu(HS)_2^-$ complex with a Cu-S bond length of 2.16 Å (Table 1), and an average S-Cu-S bond angle of 162(9)˚, in excellent agreement with the experimental results (distance 2.149(9) Å and angle 150-160˚; Etschmann et al., 2010). Simulation No. 6 (Figure 3(d)) also demonstrates that Cu(I) still forms the $Cu(HS)_2^-$ complex in the presence of 4 m sulfur (3 m HS^- and 1 m H_2S), which reveals that the maximum number of HS^- ligands around Cu(I) is 2 in hydrosulfide fluids.

The Cl-O pair distribution function can be used to compare the hydration number of free Cl^- ions with that of Cl^- ions bound to Cu(I). At a Cl-O distance of up to 4 Å, there are ~6 H_2O molecules surrounding the free Cl^- ions, while those Cl^- bound to Cu(I) are coordinated by ~5 H_2O molecules (Figure 6(a, b)). The net loss of two inner-sphere solvation waters leads to an increase in translational entropy, which favors the formation of metal complexes (Sherman, 2007, 2010). This translational entropy contribution probably plays an important role in stabilizing the $CuCl_2^-$ complex relative to CuCl(aq). The reaction

$$CuCl(aq) + Cl^- = CuCl_2^- \quad (8)$$

is actually

$$[Cu(H_2O)(Cl{\bullet}5H_2O)]^0 + (Cl{\bullet}6H_2O)^- = [Cu(Cl{\bullet}5H_2O)_2]^- + 2H_2O. \quad (9)$$

We also calculated the distribution function of the S-O pair. As shown in Figure 6(c, d), the S-O pair has a similar structure to that of the Cl-O pair, and free HS^- ions have a larger hydration number than those bound to Cu(I). At the S-O distance of 4 Å, free HS^- are surrounded by ~6 H_2O molecules, while those bound to Cu(I) are coordinated by 4 to

5 H_2O molecules; hence the grain in translational entropy upon formation of bisulfide complexes is larger than for the formation of chloride complexes.

3.2 *Ab initio* thermodynamic integration and free energy calculations

The simulations described above provide a qualitative picture of Cu(I) speciation in hydrothermal solutions. Ultimately, however, we need to obtain the thermodynamic properties of Cu complexes in order to predict their relative stabilities and the changes in the solubilities of Cu minerals in different environments and upon different processes (e.g., fluid mixing, fluid-rock interaction, phase separation).

3.2.1 Free energies for Cu-HS complexes

Figure 7 shows an example of calculating the free energy surface via distance-constrained thermodynamic integration with the simulation box containing 1 Cu^+, 1 Na^+, 2 HS^- and 55 H_2O. The Helmholtz free energy surface ($\Delta A_{a\rightarrow b}$) of the reaction:

$$Cu(HS)_2^- + H_2O = Cu(HS)(H_2O)(aq) + HS^- \qquad (10)$$

at 327 ˚C was obtained by integrating the constraint mean force with respect to the constrained Cu-S distance. As shown in Figure 7, the force is close to zero (–1.98 $kJ\cdot Å^{-1}\cdot mol^{-1}$) at 2.15 Å the distance corresponding to the equilibrated Cu-S bond length in this simulation. With increasing Cu-S distance, an external force must be applied in order to fix a given Cu-S distance because of the attraction between Cu and S. This constraint force becomes zero again at about 3.25 Å, and goes slightly positive in the range of 3.25-4.0 Å. That positive force results from the outer solvation shell and reflects the activation barrier for the ligand exchange reaction. Beyond the Cu-S distance of 4.0 Å, the force between Cu(I) and HS^- is negligible. Accounting for the size of the simulation box (length of 13.015 Å), a distance of 4.0 to 5.0 Å can be recognized as a "safe" distance beyond which the atomic interaction between the Cu(I)-HS^- pair can be neglected.

Integration of the mean constraint force along the reaction coordinates provides a free energy difference of 75.54 $kJ\cdot mol^{-1}$ for reaction 10. In the last 1 Å (4-5 Å) of the force integral, the standard deviation is 0.76 $kJ\cdot mol^{-1}$, indicating that the free energy converged. Using the same method, the free energy surfaces for the formation of the $Cu(HS)_{(aq)}$ and $Cu(HS)_2^-$ complexes at both 27 ˚C and 327 ˚C were calculated. Figure 8(a, b) shows the

integral of the free energy surfaces. Note that in order to obtain standard state free energies, activity coefficient corrections were applied as described in section 2.3.

3.2.2 Free energies for Cu-Cl complexes

The free energies for the formation of the $CuCl_x^{1-x}$ (x = 1, 2, 3) complexes were calculated in an analogous manner to those of bisulfide complexes at 27 ˚C and 327 ˚C in simulation boxes containing 1 Cu^+, 3 Na^+, 4 Cl^- and 55 H_2O. Figure 8(c, d) shows the free energy surfaces of the Cu-Cl dissociation reactions. The dissociation energies of $CuCl_{(aq)}$ and $CuCl_2^-$ at both 27 ˚C and 327 ˚C are very positive, which reflects the strong tendency of Cu(I) to react with chloride to form linear $CuCl_{(aq)}$ or $CuCl_2^-$ complexes. On the contrary, for the addition of a third Cl^-, the smaller value of free energies reflects the fact that formation of a trigonal complex with three Cl^- ligands is not favored. At 27 ˚C there is still a positive dissociation energy (12.65 kJ·mol^{-1}), so a third chloride might bind to $CuCl_2^-$ to form $CuCl_3^{2-}$. The positive dissociation energy for $CuCl_3^{2-}$ can be linked to the weak Cu-Cl bond in the $CuCl_3^{2-}$ complex at room temperature (Sherman 2007). However, at 327 ˚C, with the decrease in the free energy of the reaction, a logK of -1.23 was predicted for reaction 3, indicating that the $CuCl_3^{2-}$ species barely exists at 327 ˚C, which agrees with the unconstrained MD simulations of Sherman (2007) and with the experimental results of Brugger et al. (2007).

Based on the calculated free energies of reaction, the stability constants for the Cu-Cl and Cu-HS species were calculated according to Section 2.3. Table 2 shows the Gibbs free energies with concentration and activity corrections and the corresponding thermodynamic stability constants. $\Delta_r G$ is the Gibbs free energy of the reactions calculated from thermodynamic integration (assuming $\Delta_r G = \Delta A$), i.e. in solutions of stoichiometric ionic strengths of 2 (bisulfide) or 4 (chlorides). The errors of $\Delta_r G$ are calculated from the standard deviation of the force integral within the distance range of 4 to 5 Å. $\Delta_r G^{\Theta,c}$ is the Gibbs free energy with concentration correction calculated by equation (5), assuming unit activity coefficients. Finally, the standard state Gibbs free energies (i.e., at infinite dilution) $\Delta_r G^{\Theta}$ calculated using the activity coefficients defined by equations 5 and 6 are also shown in Table 2. The energy differences between $\Delta_r G^{\Theta,c}$ and $\Delta_r G^{\Theta}$ provide an estimate for the effect of the activity coefficients of the charged species. The $\log K^{\Theta}$ values of the reactions which form different Cu(I) complexes were calculated from equation (7) and listed in Table 2, together with selected experimental results. In most cases, the agreement is good (within one log unit).

3.2.3 Free energies for Cu-Cl-HS mixed-ligand complexes

The free energy of formation of the mixed-ligand complex $CuCl(HS)^-$ was calculated at 327 ˚C using the same method as that used for the chloride and bisulfide complexes. Since no experimental results of the mixed bisulfide-chloride system are available, we attempted to assess the precision of our calculations by comparing results from two different reaction paths (reactions 11 and 12):

$$CuCl(HS)^- = CuCl_{(aq)} + HS^- \qquad (11)$$

$$CuCl(HS)^- = CuHS_{(aq)} + Cl^- \qquad (12)$$

Since the free energies of formation for $CuCl_{(aq)}$ and $CuHS_{(aq)}$ have been calculated before, it is possible to check that these two independent reaction paths give similar results for the stability of the mixed-ligand complex.

Figure 9 shows the free energy difference of reactions 11 and 12 in forming the mixed-ligand complex. In Figure 9, the upper line gives a difference in free energy of 87.20 $kJ \cdot mol^{-1}$ between $CuCl(HS)^-$ and $CuCl_{(aq)}$ (reaction 11), and the lower line gives a difference of 44.09 $kJ \cdot mol^{-1}$ between $CuCl(HS)^-$ and $CuHS_{(aq)}$ (reaction 12). The difference of those two free energies qualitatively indicates the higher affinity of Cu(I) for the HS^- ligand relative to Cl^- under the conditions of the simulation. The logK for reactions 11 and 12 were calculated to be -7.61 and -3.85, respectively. Taking into account the formation constants of $CuCl_{(aq)}$ (logK = 3.87) and $CuHS_{(aq)}$ (logK = 7.61), the formation constant of the mixed-ligand complex, $CuCl(HS)^-$ (reaction $Cu^+ + Cl^- + HS^- = CuCl(HS)^-$) along each of the two reaction paths was obtained: logK = 11.48 (±0.46) via the reaction path $CuCl_{(aq)} \rightarrow CuCl(HS)^-$, and 11.46 (±0.17) via the reaction path $CuHS_{(aq)} \rightarrow CuCl(HS)^-$. Both values are in excellent agreement with each other, and their average, 11.47, was chosen as the formation constant of $CuCl(HS)^-$ at 327 ˚C.

3.3 Geometries of metastable Cu(I) complexes forming during distance constrained MD

Some intermediate Cu(I) complexes were observed during the distance constrained MD calculations. For example, to calculate the free energy difference between Cu^+ and $CuCl_{(aq)}$, it was necessary to constrain all the Cu-Cl distances at >=5 Å to obtain the Cu^+ aquo ion in a chloride-bearing solution. In this case, Cu(I) complexed to two H_2O molecules to form the

linear complex $Cu(H_2O)_2^+$. $Cu(H_2O)_2^+$ is metastable in solution at room temperature, disproportionating rapidly to Cu(II) and Cu(0), and hence this species has not been characterized experimentally. The geometry of $Cu(H_2O)_2^+$ and the Cu-O pair distribution function for the simulation at 327 ˚C are shown in Figure 10 (a). The Cu^+ aqua ion has a distorted linear structure with a Cu-O distance of 1.90 Å and an average O-Cu-O angle of 160(10)˚.

To form the CuCl(aq) complex for the free energy calculation of the reaction $CuCl_2^-$ = CuCl(aq) + Cl^-, three of the four Cu-Cl distances had to be constrained at distances >=5 Å (see configuration **ii** in Figure 2 (a)). The single unconstrained Cl^- was complexed to Cu(I), together with one H_2O to form the linear complex $CuCl(H_2O)$(aq). This complex presents a distorted linear structure with an average Cl-Cu-O angle of 165(6)˚ (Figure 10 (b)). The Cu-O pair distribution function gives a Cu-O distance of 1.91 Å, which is similar to the experimental value of 1.88(5) Å measured at 325 ˚C by Fulton et al. (2000b). The Cu-O bond distance and Cl-Cu-O angle are also in good agreement with the MD with only one chloride in the simulation box (Liu X et al., 2012).

The complex $CuHS(H_2O)$(aq) was formed in a box containing two HS^- ions when one Cu-S distance was constrained at 5 Å (preventing Cu-S interaction) and the other HS^- was free. The Cu-O distance in the $CuHS(H_2O)$(aq) complex was 1.98 Å, slightly longer than the Cu-O bond in the $CuCl(H_2O)$(aq) and $Cu(H_2O)_2^+$ complexes. The pair distribution function of Cu-O for the simulations containing $CuHS(H_2O)$(aq) is shown in Figure 10 (c); $CuHS(H_2O)$(aq) has a distorted linear structure with an average S-Cu-O angle of 158˚ at 327 ˚C.

4 Discussion

4.1 MD simulations vs. experiments

In this study, all the simulations were conducted with ~53 to 55 H_2O molecules plus one Cu(I) ion, a certain number of chloride and/or hydrosulfide ligands, and sodium ions to balance the charge (Table 1), which correspond to concentrations of 1 m Cu(I) with 2 to 11 m ligands. The metal species and geometries predicted by MD are in good agreement with experimental results (Table 1). The number of ligands bonded to Cu(I) is limited due to steric

effects. Cu(I) is a good example of the steric differences between solutions and solids; while Cu(I) in solids is overwhelmingly tetrahedrally coordinated with Cl, in solution linear Cu(I) chloride complexes are formed, as well as small amounts of trigonal planar complexes at low temperature (Brugger et al. 2007; Sherman 2007). The free energy surface determined in our *ab initio* MD simulations allows us to interpret the coordination number of Cu(I) complexes accurately. For instance, the positive free energy of forming $CuCl_3^{2-}$ complexes at high temperature indicates quantitatively that this complex is not significant under these conditions.

The metal concentrations in these MD simulations are high compared to the concentrations in natural fluids (Liu W et al., 2008; Seward and Barnes, 1997; Sherman, 2007; Etschmann et al., 2010). To reproduce the lower concentrations of real fluids, more H_2O molecules are needed in the simulation box to dilute the metal and ligand ions. For example, a simulation box with one Cu^+ and 1110 H_2O is required to simulate a fluid containing 0.05 m Cu^+. That kind of simulation is currently achievable routinely in classical MD (Driesner et al., 1998; Harris et al., 2001; Sherman, 2001; 2010; Sherman and Collings, 2002); however, in *ab initio* MD, it is very costly in terms of CPU time (Hutter and Curioni, 2005). In this study, for a typical MD simulation with 173 atoms and a box length of 13.066 Å, it took ~16 hours to obtain one picosecond by parallel calculations using 24 cores. For the simulation with 185 atoms and box length of 13.534 Å, it took ~24 hours to calculate one picosecond (using 24 cores). A small increase in particle number and box size can lead to a dramatic increase of CPU time. Therefore, it is not (yet) realistic to simulate dilute fluids via *ab inito* MD, especially for methods such as thermodynamic integration. On the other hand, since periodic boxes were employed in the *ab initio* MD simulations, the Cu-Cu interaction is negligible, and Cu can be considered to be at infinite dilution with respect to Cu-Cu interactions. This approach has been widely used in many *ab initio* MD studies of low concentration metal ions in aqueous solutions (e.g., Ayala et al. 2010; Beret et al., 2008; Terrier et al. 2010).

4.2 Entropy and complex formation

Based on the predicted stable Cu(I) species in different solutions (Table 1), the order of affinity ligands for forming complexes with Cu(I) is $HS^- > Cl^- > H_2S(aq)$. This is in agreement with the previous experimental results that suggest that the Cu-HS complexes are stronger than Cu-Cl complexes (Etschmann et al. 2010; Mountain and Seward, 2003). Under

hydrothermal conditions, the number of Cl^- or HS^- ligands around Cu^+ was found to be 2. The loss of hydration water of Cl^- or HS^- upon complexation with Cu(I) (Figure 6) is the likely driving force for the formation of these fully coordinated metal complexes (Sherman 2007). Including the hydration water in the ion exchange reactions, the complexing of the Cu(I) aqua ion can be written as:

$$Cu(H_2O)_2^+ + [Cl(H_2O)_m]^- = Cu(H_2O)(Cl(H_2O)_n) + (m+1-n)\,H_2O \quad (13)$$

$$Cu(H_2O)_2^+ + [HS(H_2O)_m]^- = Cu(H_2O)(HS(H_2O)_n) + (m+1-n)\,H_2O \quad (14)$$

In addition to one water molecule that is replaced by a chloride or bisulfide ion, additional water is released because of the lower hydration number of the ligands when complexed to Cu(I) (i.e., m>n in equations 13 and 14). So, halide and bisulfide complexing render the system more disordered, and the entropy increases during this process, which makes the replacement of a water ligand by a Cl^- or a HS^- energetically advantageous. Figures 6 (a, b) and (c, d) show that the loss of hydration water (m-n) is ~1 for Cl^-, and this number is larger for HS^- (~1 to 2). The free energy surfaces of the ion exchange reactions show larger energy gains for forming Cu-HS complexes compared to Cu-Cl complexes, which is (at least partly) due to the higher loss of hydration waters for HS^-.

4.3 Thermodynamic properties

The thermodynamic properties of Cu(I) complexes were calculated via thermodynamic integration (Table 2). In many experimental studies (e.g, Mountain and Seward, 1999, 2003; Xiao et al., 1998), the formation constants of Cu(I) complexes were measured at saturated water vapor pressure over limited ranges in temperature; for comparison, we use the equation of states fit to the experimental data by different authors (see Figs. 11,12). The predicted stability constants for Cu-Cl and Cu-HS complexes are in good agreement with recent experimental values (Table 2), and in most cases, the differences between simulated and experimental data are within 1-2 log units. At lower temperature, the free energies of the second-step association of the $Cu(HS)_2^-$ and $CuCl_2^-$ complexes are relatively higher than the experimental values. A major source of this discrepancy is that the kinetics of ion exchange is faster at higher temperature, so it will take longer to explore all the configurations and get the average constraint force at room temperature. Because thermodynamic integration needs very large computing time and resources, it would be too time-consuming to calculate for much longer than ~10 ps for each constrained mean force.

It is important to realize that the experimental uncertainty on the formation constants of metal complexes at elevated P and T is relatively large, and that agreement within about one

order of magnitude for the dissociation constant provides very useful information. Figure 11 compares the $\log K^{\theta}$ of Cu-Cl and Cu-HS complexes based on different experimental studies (Akinfiev and Zotov, 2001; Brugger et al., 2007; Liu W and McPhail, 2005; Liu W et al., 2001; Mountain and Seward, 1999; 2003; Xiao et al., 1998) as a function of temperature, with the predicted $\log K^{\theta}$ by MD simulations. Discrepancies of around one logK unit among different experimental studies are common, and indeed thermodynamic integration shows good potential to predict thermodynamic properties under wide range of conditions. In the following section, we show that MD data enable realistic predictions of the behavior of Cu(I) in hydrothermal solutions.

4.4 Geological implications

As the formation constants of $CuCl(HS)^-$ and other Cu(I) chloride and bisulfide complexes have been calculated through MD simulations, we can now construct an activity-activity diagram which considers the mixed-ligand complex. Figure 12 compares the mineral solubility (Cu-S-H_2O system) and predominance fields of Cu(I) species as a function of Cl^- and HS^- activities at 325 ˚C, 500 bar (pH = 5, and $\log f_{O2}$ of -35). Figure 12(a) is based on the available properties derived from experimental studies (referred to from now on as *experiment-based*) (Brugger et al., 2007; Liu W and McPhail, 2005; Mountain and Seward, 2003), while Figure 12(b) is calculated entirely based on the formation constants of Cu(I) aqueous species generated by the MD simulations (*MD-based*) (Table 2).

Compared with the speciation predicted using stability constants fit to experimental data (Figure 12(a)), the speciation based on the stability constants derived here suggest that the $CuCl_{(aq)}$ and $Cu(HS)_{(aq)}$ complexes are not significant in ore-forming fluids (Figure 12(b)). Moreover, the mixed-ligand complex $CuCl(HS)^-$ has a wide predominance field (Figure 12(b)), implying that this species is likely to play an important role in Cu transport in hydrothermal fluids.

Given our estimates of the stability constant of the mixed-ligand complexes, we can also estimate the effect of this complex on the solubilities of Cu minerals in hydrothermal fluids. Figure 13 shows a simple simulation where Cu phases precipitate and dissolve as HS^- is added to a closed system consisting of 1 kg of water containing 3 m Cl_{tot}, 10^{-15} m S_{tot}, 5 000 mg/kg Cu^+, and 10 000 mg/kg Fe^{2+}. The $pH_{325°C}$ of 6 was chosen as it is consistent with the K-feldspar-Muscovite-Quartz buffer (~$pH_{325\,°C}$ =5.5-4.5 for activities of K^+ between 0.001 and 0.1) and the HS^-/H_2S buffer ($pK_{a,325°C}$ ~ 7). A $\log f_{O2}$ value of -31 was chosen to keep

sulfur in its reduced state (predominantly HS^- and H_2S(aq)). Sodium was added to balance the charges in the initial solution. The calculated stable mineral phases in equilibrium with the initial (i.e., essentially S-free) fluid are native copper, magnetite and chalcocite. The concentrations of the aqueous Cu species (Cu solubility corresponds to the concentration of the predominant species on the logarithmic scale of the diagram) are shown as a function of the reacted HS^- (similar to total sulfur concentration) based on both experiment-based log Ks (Figure 13 (a)) and MD-based log Ks (Figure 13 (b)) for Cu(I) chloride and bisulfide complexes. In general, the qualitative predictions of the models based on experimental and MD data are consistent with each other, both predicting high Cu solubility at low (< 0.05 m) or high (>0.4 m) S concentrations, with a minimum in solubility in the intermediate region. Identifying such solubility gradients is one of the primary aims of reactive transport modeling. Another important aim of the modeling is to constrain conditions under which significant amounts of metals can be mobilized. The mineral solubilities predicted using both sets of thermodynamic properties agree qualitatively, although the MD model predicts higher Cu concentrations (1000's instead of 100's of ppm). Such high concentrations have indeed been found in natural fluid inclusions (e.g., Cauzid et al. 2007; Audétat et al. 1998). The stability constants derived from fits to experimental data predict that fluids with intermediate S contents (0.05-0.4 m) have no ability to carry Cu (< 5 ppm); however, the stability constants derived here predict that significant Cu (~100 ppm) still remains in solutions as the mixed-ligand complex $CuCl(HS)^-$. Under these conditions, the mineral assemblage consists of magnetite-chalcopyrite-chalcocite-bornite, or magnetite-chalcopyrite-pyrrhotite (Figures 13a, d). These mineral assemblages are commonly found in magmatic hydrothermal copper deposits (e.g., the giant Olympic Dam Fe oxide Cu-Au deposits, Haynes et al., 1995). Recent ICP-MS measurement of single fluid inclusions show that sulfur concentration ranges from 0.1 to 0.55 m in magmatic hydrothermal ore fluids (e.g., 0.24 m at 323 ˚C for Bingham Canyon Cu-Au-Mo porphyry deposit, USA, Seo et al., 2009). Therefore, it is quite possible that the mixed-ligand complex $CuCl(HS)^-$ can transport significant copper in such ore fluids.

Acknowledgement: Research funding was provided by Australian Research Council (ARC) to JB (DP0878903), and the Minerals Down Under Flagship to WL. The MD calculations were supported by iVEC through the use of advanced computing resources located in Perth, Australia, and the computational facilities of the Advanced Computing Research Centre in University of Bristol, UK. This paper is part of Yuan Mei's PhD thesis. YM acknowledges

the University of Adelaide for IPRS scholarship and CSIRO Minerals Down Under Flagship for a scholarship top-up. The authors are also grateful for the helpful comments of Edwin Schauble (Associate Editor) and three anonymous reviewers.

References

Akinfiev, N. N. and Zotov, A. V., 2001. Thermodynamic description of chloride, hydrosulfide, and hydroxo complexes of Ag(I), Cu(I), and Au(I) at temperatures of 25-500°C and pressures of 1-2000 bar. *Geochemistry International* **39**, 990-1006.

Alessandro, L. and Francesco, L. G., 2008. Metadynamics: a method to simulate rare events and reconstruct the free energy in biophysics, chemistry and material science. *Reports on Progress in Physics* **71**, 126601.

Archibald, S. M., Migdisov, A. A., and Williams-Jones, A. E., 2002. An experimental study of the stability of copper chloride complexes in water vapor at elevated temperatures and pressures. *Geochimica et Cosmochimica Acta* **66**, 1611-1619.

Audétat, A., Günther, D., and Heinrich, C. A., 1998. Formation of a magmatic-hydrothermal ore deposit: insights with LA-ICP-MS analysis of fluid inclusions. Science 279, 2091-279.

Ayala, R., Spezia, R., Vuilleumier, R., Martínez, J. M., Pappalardo, R. R., and Sánchez Marcos, E., 2010. An Ab Initio Molecular Dynamics Study on the Hydrolysis of the Po(IV) Aquaion in Water. The Journal of Physical Chemistry B 114, 12866-12874.

Berendsen, H. J. C., Grigera, J. R., and Straatsma, T. P., 1987. The missing term in effective pair potentials. *The Journal of Physical Chemistry* **91**, 6269-6271.

Beret, E. C., Martínez, J. M., Pappalardo, R. R., Marcos, E. S., Doltsinis, N. L., and Marx, D., 2008. Explaining asymmetric solvation of Pt(II) versus Pd(II) in aqueous solution revealed by *ab initio* molecular dynamics simulations. *Journal of Chemical Theory and Computation* 4, 2108-2121.

Bethke, C.M., 2008, *Geochemical and biogeochemical reaction modeling (second edition)*: New York, Cambridge University Press, 564 p.

Borisov, M. V., and Shvarov, Yu. V., 1992, *Thermodynamics of geochemical processes*: Moscow, Moscow State University Publishing House, 254 p. (in Russian).

Brugger, J., Etschmann, B., Liu, W., Testemale, D., Hazemann, J. L., Emerich, H., van Beek, W., and Proux, O., 2007. An XAS study of the structure and thermodynamics of Cu(I) chloride complexes in brines up to high temperature (400˚C, 600 bar). *Geochimica et Cosmochimica Acta* **71**, 4920-4941.

Brugger, J., Pring, A., Reith, F., Ryan, C., Etschmann, B., Liu, W., O'Neill, B., and Ngothai, Y., 2010. Probing ore deposits formation: new insights and challenges from synchrotron and neutron studies. *Radiation Physics and Chemistry* **79**, 151-161.

Bühl, M. and Grenthe, I., 2011. Binding modes of oxalate in UO_2 (oxalate) in aqueous solution studied with first-principles molecular dynamics simulations. Implications for the chelate effect. *Dalton Trans.* **40**, 11192-11199.

Bühl, M. and Golubnychiy, V., 2007. Binding of pertechnetate to uranyl(VI) in aqueous solution. A density functional theory molecular dynamics study. *Inorganic Chemistry* **46**, 8129-8131.

Bühl, M., Kabrede, H., Diss, R., and Wipff, G., 2006. Effect of hydration on coordination properties of uranyl(VI) complexes. A first-principles molecular dynamics study. *Journal of the American Chemical Society* **128**, 6357-6368.

Bühl, M., Sieffert, N., Golubnychiy, V., and Wipff, G., 2008. Density functional theory study of uranium(VI) aquo chloro complexes in aqueous solution. *The Journal of Physical Chemistry A* **112**, 2428-2436.

Car, R. and Parrinello, M., 1985. Unified approach for molecular dynamics and density-functional theory. *Physical Review Letters* **55**, 2471-2474.

Cauzid, J., Philippot, P., Martinez-Criado, G., Menez, B., and Laboure, S., 2007. Contrasting Cu-complexing behaviour in vapour and liquid fluid inclusions from the Yankee Lode tin deposit, Mole Granite, Australia. Chemical Geology 246, 39-54.

Crerar, D. A. and Barnes, H. L., 1976. Ore solution chemistry V. Solubilities of chalcopyrite and chalcocite assemblages in hydrothermal solution at 200 degree to 350 degree C. *Economic Geology* **71**, 772-794.

D'Angelo, P., Barone, V., Chillemi, G., Sanna, N., Meyer-Klaucke, W., and Pavel, N. V., 2002. Hydrogen and higher shell contributions in Zn^{2+}, Ni^{2+}, and Co^{2+} aqueous solutions: an X-ray absorption fine structure and molecular dynamics study. *Journal of the American Chemical Society* **124**, 1958-1967.

D'Angelo, P., Roscioni, O. M., Chillemi, G., Della Longa, S., and Benfatto, M., 2006. Detection of Second Hydration Shells in Ionic Solutions by XANES: Computed spectra for Ni^{2+} in water based on molecular dynamics. *Journal of the American Chemical Society* **128**, 1853-1858.

Dang, L. X., Schenter, G. K., Glezakou, V.-A., and Fulton, J. L., 2006. Molecular simulation analysis and X-ray absorption mMeasurement of Ca^{2+}, K^{+} and Cl^{-} ions in solution. *The Journal of Physical Chemistry B* **110**, 23644-23654.

Driesner, T., 2007. The system H_2O–NaCl. Part II: Correlations for molar volume, enthalpy, and isobaric heat capacity from 0 to 1000 °C, 1 to 5000 bar, and 0 to 1 X_{NaCl}. *Geochimica et Cosmochimica Acta* **71**, 4902-4919.

Driesner, T. and Heinrich, C. A., 2007. The system H_2O–NaCl. Part I: Correlation formulae for phase relations in temperature–pressure–composition space from 0 to 1000°C, 0 to 5000bar, and 0 to 1 XNaCl. *Geochimica et Cosmochimica Acta* **71**, 4880-4901.

Driesner, T., Seward, T. M., and Tironi, I. G., 1998. Molecular dynamics simulation study of ionic hydration and ion association in dilute and 1 molal aqueous sodium chloride solutions from ambient to supercritical conditions. *Geochimica et Cosmochimica Acta* **62**, 3095-3107.

Etschmann, B. E., Black, J., Grundler, P., Borg, S., Brewe, D., McPhail, D. C., Spiccia, L., and Brugger, J., 2011. Copper(I) speciation in mixed thiosulfate-chloride and ammonia-chloride solutions: XAS and UV-Visible spectroscopic studies. *RSC Advances* **1**, 1554-1566.

Etschmann, B. E., Liu, W., Testemale, D., Müller, H., Rae, N. A., Proux, O., Hazemann, J. L., and Brugger, J., 2010. An in situ XAS study of copper(I) transport as hydrosulfide complexes in hydrothermal solutions (25-592 °C, 180-600 bar): Speciation and solubility in vapor and liquid phases. *Geochimica et Cosmochimica Acta* **74**, 4723-4739.

Fritz, J. J., 1980. Chloride complexes of copper(I) chloride in aqueous solution. *The Journal of Physical Chemistry* **84**, 2241-2246.

Fritz, J. J., 1981. Representation of the solubility of copper(I) chloride in solutions of various aqueous chlorides. *The Journal of Physical Chemistry* **85**, 890-894.

Fulton, J. L., Hoffmann, M. M., Darab, J. G., Palmer, B. J., and Stern, E. A., 2000a. Copper(I) and copper(II) coordination structure under hydrothermal conditions at 325 °C: An X-ray absorption fine structure and molecular dynamics study. *The Journal of Physical Chemistry A* **104**, 11651-11663.

Fulton, J. L., Hoffmann, M. M., and Darab, J. G., 2000b. An X-ray absorption fine structure study of copper(I) chloride coordination structure in water up to 325°C. *Chemical Physics Letters* **330**, 300-308.

Fulton, J. L., Kathmann, S. M., Schenter, G. K., and Balasubramanian, M., 2009. Hydrated structure of Ag(I) ion from symmetry-dependent, K- and L-edge XAFS multiple scattering and molecular dynamics simulations. *The Journal of Physical Chemistry A* **113**, 13976-13984.

Guymon, C. G., Harb, J. N., Rowley, R. L., and Wheeler, D. R., 2008. MPSA effects on copper electrodeposition investigated by molecular dynamics simulations. *The Journal of Chemical Physics* **128**, 044717.

Habershon, S. and Manolopoulos, D. E., 2011. Free energy calculations for a flexible water model. *Physical Chemistry Chemical Physics*.

Haile, J. M., 1992. *Molecular dynamics simulation : elementary methods*. Wiley, New York

Harris, D. J., Brodholt, J. P., Harding, J. H., and Sherman, D. M., 2001. Molecular dynamics simulation of aqueous $ZnCl_2$ solutions. *Molecular Physics* **99**, 825-833.

Harris, D. J., Brodholt, J. P., and Sherman, D. M., 2003. Zinc complexation in hydrothermal chloride brines: Results from ab initio molecular dynamics calculations. *Journal of Physical Chemistry A* **107**, 1050-1054.

Haynes, D. W., Cross, K. C., Bills, R. T., and Reed, M. H., 1995. Olympic Dam ore genesis; a fluid-mixing model. *Economic Geology* **90**, 281-307.

Helgeson, H. C., 1969. Thermodynamics of hydrothermal systems at elevated temperatures and pressures. *American Journal of Science* **267**, 729-804.

Helgeson, H. C. and Kirkham, D. H., 1974. Theoretical prediction of the thermodynamic behavior of aqueous electrolytes at high pressures and temperatures; II, Debye-Huckel parameters for activity coefficients and relative partial molal properties. *American Journal of Science* **274**, 1199-1261.

Helgeson, H. C., Kirkham, D. H., and Flowers, G. C., 1981. Theoretical prediction of the thermodynamic behavior of aqueous electrolytes by high pressures and temperatures; IV, Calculation of activity coefficients, osmotic coefficients, and apparent molal and standard and relative partial molal properties to 600 degrees C and 5kb. *American Journal of Science* **281**, 1249-1516.

Hemley, J. J., Cygan, G. L., Fein, J. B., Robinson, G. R., and d'Angelo, W. M., 1992. Hydrothermal ore-forming processes in the light of studies in rock-buffered systems; I, Iron-copper-zinc-lead sulfide solubility relations. *Economic Geology* **87**, 1-22.

Hoffmann, M. M., Darab, J. G., Palmer, B. J., and Fulton, J. L., 1999. A transition in the Ni^{2+} complex structure from six- to four-coordinate upon formation of ion pair species in supercritical water: An X-ray absorption fine structure, near-infrared, and molecular dynamics study. *Journal of Physical Chemistry* **103**, 8471-8482.

Hutter, J. and Curioni, A., 2005. Car–Parrinello Molecular Dynamics on Massively Parallel Computers. *ChemPhysChem* **6**, 1788-1793.

John P, B., 1998. Molecular dynamics simulations of aqueous NaCl solutions at high pressures and temperatures. *Chemical Geology* **151**, 11-19.

Laasonen, K., Pasquarello, A., Car, R., Lee, C., and Vanderbilt, D., 1993. Car-Parrinello molecular dynamics with Vanderbilt ultrasoft pseudopotentials. *Physical Review B* **47**, 10142-10153.

Laio, A. and Parrinello, M., 2002. Escaping free-energy minima. *Proceedings of the National Academy of Sciences* **99**, 12562-12566.

Lin, I. C., Seitsonen, A. P., Tavernelli, I., and Rothlisberger, U., 2012. Structure and Dynamics of Liquid Water from ab Initio Molecular Dynamics—Comparison of

BLYP, PBE, and revPBE Density Functionals with and without van der Waals Corrections. *Journal of Chemical Theory and Computation* **8**, 3902-3910.

Liu, W., Borg, S., Etschmann, B., Mei, Y., and Brugger, J., 2012. An XAS study of speciation and thermodynamic properties of aqueous zinc bromide complexes at 25-150 ˚C. *Chemical Geology*.

Liu, W., Brugger, J., Etschmann, B., Testemale, D., and Hazemann, J.-L., 2008. The solubility of nantokite (CuCl(s)) and Cu speciation in low-density fluids near the critical isochore: An in-situ XAS study. *Geochimica et Cosmochimica Acta, 2008; 72(16):4094-4106 10.1016/j.gca.2008.05.056*.

Liu, W., Brugger, J., McPhail, D. C., and Spiccia, L., 2002. A spectrophotometric study of aqueous copper(I)-chloride complexes in LiCl solutions between 100˚C and 250˚C. *Geochimica et Cosmochimica Acta* **66**, 3615-3633.

Liu, W., Etschmann, B., Foran, G., Shelly, M., Foran, G., and Brugger, J., 2007. Deriving formation constants for aqueous metal complexes from XANES spectra: Zn(II) and Fe(II) chloride complexes in hypersaline solutions. *American Mineralogist* **92**, 761-770.

Liu, W., McPhail, D. C., and Brugger, J., 2001. An experimental study of copper(I)-chloride and copper(I)-acetate complexing in hydrothermal solutions between 50˚C and 250˚C and vapor-saturated pressure. . *Geochimica et Cosmochimica Acta* **65**, 2937-2948.

Liu, W. and McPhail, D. C., 2005. Thermodynamic properties of copper chloride complexes and copper transport in magmatic-hydrothermal solutions. *Chemical Geology* **221**, 21-39.

Liu, X., Lu, X., Jan Meijer, E., and Wang, R., 2010a. Hydration mechanisms of Cu^{2+}: Tetra-, penta- or hexa-coordinated? *Physical Chemistry Chemical Physics* **12**, 10801-10804.

Liu, X., Lu, X., Meijer, E. J., Wang, R., and Zhou, H., 2010b. Acid dissociation mechanisms of $Si(OH)_4$ and $Al(H_2O)_6^{3+}$ in aqueous solution. *Geochimica et Cosmochimica Acta* **74**, 510-516.

Liu, X., Lu, X., Wang, R., and Meijer, E. J., 2011a. Understanding hydration of Zn^{2+} in hydrothermal fluids with ab initio molecular dynamics. *Physical Chemistry Chemical Physics* **13**, 13305-13309.

Liu, X., Lu, X., Wang, R., and Zhou, H., 2012. Silver speciation in chloride-containing hydrothermal solutions from first principles molecular dynamics simulations. *Chemical Geology* **294–295**, 103-112.

Liu, X., Lu, X., Wang, R., Zhou, H., and Xu, S., 2011b. Speciation of gold in hydrosulphide-rich ore-forming fluids: Insights from first-principles molecular dynamics simulations. *Geochimica et Cosmochimica Acta* **75**, 185-194.

Mambote, R. C. M., Krijgsman, P., and Reuter, M. A., 2003. Hydrothermal precipitation of arsenic compounds in the ferric–arsenic (III)–sulfate system: thermodynamic modeling. *Minerals Engineering* **16**, 429-440.

Mangold, M., Rolland, L., Costanzo, F., Sprik, M., Sulpizi, M., and Blumberger, J., 2011. Absolute pKa Values and Solvation Structure of Amino Acids from Density Functional Based Molecular Dynamics Simulation. *Journal of Chemical Theory and Computation* **7**, 1951-1961.

Mavrogenes, J. A., Berry, A. J., Newville, M., and Sutton, S. R., 2002. Copper speciation in vapor-phase fluid inclusions from the Mole Granite, Australia. *American Mineralogist* **87**, 1360-1364.

Mountain, B. W. and Seward, T. M., 1999. The hydrosulphide/sulphide complexes of copper(I): experimental determination of stoichiometry and stability at 22˚C and reassessment of high temperature data. *Geochimica et Cosmochimica Acta* **63**, 11-29.

Mountain, B. W. and Seward, T. M., 2003. Hydrosulfide/sulfide complexes of copper(I): Experimental confirmation of the stoichiometry and stability of $Cu(HS)_2^-$ to elevated temperatures. *Geochimica et Cosmochimica Acta* **67**, 3005-3014.

Perdew, J. P., Burke, K., and Ernzerhof, M., 1996. Generalized Gradient Approximation Made Simple. *Physical Review Letters* **77**, 3865-3868.

Pokrovski, G. S., Tagirov, B. R., Schott, J., Hazemann, J.-L., and Proux, O., 2009. A new view on gold speciation in sulfur-bearing hydrothermal fluids from in situ X-ray absorption spectroscopy and quantum-chemical modeling. *Geochimica et Cosmochimica Acta* **73**, 5406-5427.

Resat, H. M., Mihaly, 1993. Studies on free energy calculations. I. Thermodynamic integration using a polynomial path. *The Journal of Chemical Physics* **99**, 6052-6061.

Seward, T. M. and Barnes, H. L., 1997. Metal transport by hydrothermal ore fluids. In: Barnes, H. L. (Ed.), *Geochemistry of Hydrothermal Ore Deposits*. Wiley, New York.

Seward, T. M. and Driesner, T., 2004. Hydrothermal solution structure: experiments and computer simulations. In: Palmer, D. A., Fernández-Prini, R., and Havey, A. H. Eds.), *Aqueous systems at elevated temperatures and pressures: physical chemistry in water, steam and hydrothermal solutions*. Elsevier.

Seo, J. H., Guillong, M., and Heinrich, C. A., 2009. The role of sulfur in the formation of magmatic-hydrothermal copper-gold deposits. Earth and Planetary Science Letters 282, 323-328.

Seyfried Jr, W. E. and Ding, K., 1993. The effect of redox on the relative solubilities of copper and iron in Cl-bearing aqueous fluids at elevated temperatures and pressures: An experimental study with application to subseafloor hydrothermal systems. *Geochimica et Cosmochimica Acta* **57**, 1905-1917.

Sherman, D. M., 2001. Quantum Chemistry and Classical Simulations of Metal Complexes in Aqueous Solutions. *Reviews in Mineralogy and Geochemistry* **42**, 273-317.

Sherman, D. M., 2007. Complexation of Cu^+ in Hydrothermal NaCl Brines: Ab initio molecular dynamics and energetics. *Geochimica et Cosmochimica Acta* **71**, 714-722.

Sherman, D. M., 2010. Metal complexation and ion association in hydrothermal fluids: insights from quantum chemistry and molecular dynamics. *Geofluids* **10**, 41-57.

Sherman, D. M. and Collings, M. D., 2002. Ion association in concentrated NaCl brines from ambient to supercritical conditions: results from classical molecular dynamics simulations. *Geochemical Transactions* **3**, 102-107.

Smith, D. E. and Dang, L. X., 1994. Computer simulations of NaCl association in polarizable water. *The Journal of Chemical Physics* **100**, 3757-3766.

Sprik, M. C., Giovanni, 1998. Free energy from constrained molecular dynamics. *Journal of Chemical Physics* **109**, 7737-7744.

Sverjensky, D., Shock, E., and Helgeson, H., 1997. Prediction of the thermodynamic properties of aqueous metal complexes to 1000 C and 5 kb. *Geochimica et Cosmochimica Acta* **61**, 1359-1412.

Terrier, C., Vitorge, P., Gaigeot, M.-P., Spezia, R., and Vuilleumier, R., 2010. Density functional theory based molecular dynamics study of hydration and electronic properties of aqueous La^{3+}. *The Journal of Chemical Physics* **133**, 044509.

van Sijl, J., Allan, N. L., Davies, G. R., and van Westrenen, W., 2010. Titanium in subduction zone fluids: First insights from ab initio molecular metadynamics simulations. *Geochimica et Cosmochimica Acta* **74**, 2797-2810.

Var'yash, L. N., 1992. Cu(I) complexing in NaCl solutions at 300 and 350 ˚C. *Geochemistry International* **29**, 84-92.

Xiao, Z., Gammons, C. H., and Williams-Jones, A. E., 1998. Experimental study of copper(I) chloride complexing in hydrothermal solutions at 40 to 300 ˚C and saturated water

vapor pressure. *Geochimica et Cosmochimica Acta* **62**, 2949-2964.

Zeng, X., Hu, H., Hu, X., Cohen, A. J., and Yang, W., 2008. Ab initio quantum mechanical/molecular mechanical simulation of electron transfer process: fractional electron approach. *Journal of Chemical Physics* **128**, 124510.

Table 1. Details of simulated Cu-Cl-HS/H_2S solutions at 327 ˚C, and resulting geometries of the predicted Cu(I) complexes.

No.	Amount of water and ligands	Box size (Å)	Density (g/cm^3)	Equilibrium species	Cu-Cl distance		Cu-S distance		Angle (˚)	
					This study	Exp.	This study	Exp.	This study	Exp.
1	$53H_2O$, $1Cu^+$, $3Na^+$, $4Cl^-$, $2H_2S$	13.066	0.9660	$CuCl_2^-$	2.13	2.152(7) [1]	-	-	163.66	161.5[1]
2	$53H_2O$, $1Cu^+$, $4Na^+$, $4Cl^-$, $1H_2S$, $1HS^-$	13.066	0.9823	$CuCl(HS)^-$	2.15	-	2.14	-	162.03	-
3	$53H_2O$, $1Cu^+$, $5Na^+$, $4Cl^-$, $2HS^-$	13.066	0.9987	$CuCl(HS)^-$	2.17	-	2.16	-	162.58	-
4	$54H_2O$, $1Cu^+$, $10Na^+$, $10Cl^-$, $1HS^-$	13.534	1.108	$CuCl(HS)^-$ $CuCl_2(HS)^-$	2.16	-	2.16	-	163.48§	-
5	$55H_2O$, $1Cu^+$, $1Na^+$, $2HS^-$	13.015	0.8615	$Cu(HS)_2^-$	-	-	2.16	2.149[2]	161.95	157[2]
6	$53H_2O$, $1Cu^+$, $2Na^+$, $3HS^-$, $1H_2S$	13.015	0.9023	$Cu(HS)_2^-$	-	-	2.15	2.149[2]	163.91	157[2]

* Box size indicates the length of cubic boxes of simulations.
§ Bond angle of Cl-Cu-S for $CuCl(HS)^-$.
References: [1] Brugger et al. (2007); [2] Etschmann et al. (2010).

Table 2. Gibbs free energy of reaction and stability constants of the Cu-Cl and Cu-HS association reactions.

Reaction	T (°C)	$\Delta_r G$ (kJ/mol)	$\Delta_r G^{\theta,c}$ (kJ/mol)	$\Delta_r G^{\theta}$ (kJ/mol)	log K	Experiment results
$Cu^+ + Cl^- = CuCl\,(aq)$	27	-25.1 (±0.8)	-19.5	-18.1	3.15±0.13	4.13[1]
$CuCl\,(aq) + Cl^- = CuCl_2^-$	27	-27.1 (±1.3)	-22.3	-22.5	3.92±0.23	1.32[1]
$CuCl_2^- + Cl^- = CuCl_3^{2-}$	27	-12.7 (±2.0)	-9.2	-6.2	1.07±0.34	-0.69[1]
$Cu^+ + Cl^- = CuCl\,(aq)$	327	-41.3 (±1.6)	-30.0	-44.5	3.87±0.14	4.12[1]
$CuCl\,(aq) + Cl^- = CuCl_2^-$	327	-41.2 (±1.0)	-31.7	-32.6	2.84±0.09	1.98[1]
$CuCl_2^- + Cl^- = CuCl_3^{2-}$	327	-3.3 (±2.4)	3.6	14.1	-1.23±0.21	-2.17[1]
$Cu^+ + HS^- = CuHS\,(aq)$	27	-70.2 (±0.7)	-66.8	-67.5	11.75±0.12	12.56[2]
$CuHS\,(aq) + HS^- = Cu(HS)_2^-$	27	-53.9 (±1.2)	-53.9	-54.0	9.40±0.20	4.72[2]
$Cu^+ + HS^- = CuHS\,(aq)$	327	-81.9 (±1.5)	-75.0	-87.5	7.61±0.13	8.02[2]
$CuHS\,(aq) + HS^- = Cu(HS)_2^-$	327	-75.5 (±0.8)	-75.5	-76.2	6.64±0.07	3.61[2]
$CuHS\,(aq) + Cl^- = CuCl(HS)^-$	327	-43.4 (±0.6)	-43.4	-44.1	3.85±0.04	
$CuCl\,(aq) + HS^- = CuCl(HS)^-$	327	-86.5 (±3.7)	-86.5	-87.2	7.61±0.32	

$\Delta_r G$: Gibbs free energy for the reaction; $\Delta_r G^{\theta,c}$: Gibbs free energy at infinite dilution, calculated assuming unit activity coefficients; $\Delta_r G^{\theta}$: Gibbs free energy at infinite dilution, with concentration and activity correction.
[1] Calculated using HKF parameters fitted by Brugger et al. (2007) and Liu W et al. (2001).
[2] Calculated using a Ryzhenko model (Borisov, and Shvarov, 1992) based on the experimental data by Moutain and Seward (1999, 2003).

Figure Captions

Figure 1. Constraint forces versus running average for constrained MD simulation of Cu-Cl at 327 ˚C by constraining Cu-Cl distances at 4.25, 6.00, 6.00, 6.00 Å, respectively. The geometry shows that Cu(I) formed the aqueous complex $Cu(H_2O)_2^+$ by complexing with two water molecules. The line with fluctuation is the constraint forces (kJ $Å^{-1}$ mol^{-1}), and the line in the middle is the running average.

Figure 2. Reaction paths and constrained distances from for a ligand substitution reaction (a) and a ligand addition reaction (b). **Configuration i** indicates the reactants of and **configuration ii** indicates the products of each reaction. The dashed lines show the constrained Cu-Cl bond at long distances, the solid lines show the constrained Cu-Cl bonds along the reaction path, and the solid bonds with atom color are the unconstrained Cu-Cl bonds.

Figure 3. Cu-Cl and Cu-S distances vs. simulation time at 327 ˚C (500 bar).

Figure 4. Cu-Cl pair distribution functions (solid lines) and their integrals (number of Cl atoms surrounding the Cu centre; dashed lines).

Figure 5. Cu-S pair distribution functions (solid lines) and their integrals (number of S atoms surrounding the Cu centre; dashed lines)

Figure 6. Hydration number of chloride and sulfur atoms. Pair distribution functions for Cl-O (a and b) and S-O (c and d) are shown with solid lines, and their integrals (showing the hydration numbers) with dashed lines. In each diagram, the thick lines correspond to the hydration around free Cl^- or HS^- ions, while the thin lines refer to the hydration of Cl^- or HS^- ions bonded to Cu^+.

Figure 7. An example of constrained mean forces (empty circles) and their integration (solid circles) for the reaction $Cu(HS)_2^- + H_2O = Cu(HS)(H_2O)(aq) + HS^-$. The empty circles are the running averages of constraint forces at each distance, and the solid circles are the numerical integrals of the mean constraint force with respect to the distance. The Cu-S bond lengths were changed from 2.15 Å (configuration **a, reactants**) to 5.0 Å (configuration **b, products**).

Figure 8. Free energy surfaces of Cu-HS (a and b) and Cu-Cl (c and d) complexes at 27˚C and 327˚C.

Figure 9. Free energy surfaces of the $CuCl(HS)^-$ mixed ligand complex at 327 ˚C.

Figure 10. Geometries, bond angles and Cu-O pair distribution functions of metastable Cu(I) aqueous species in the distance-constraint simulations at 327 ˚C.

Figure 11. Formation constants of Cu-Cl and Cu-HS complexes by MD simulation versus those derived from experiments. For Cu-Cl complexes, the solid line is calculated from HKF parametes by Brugger et al. (2007) and Liu W and McPhail (2005), the dotted line is fitted from Xiao et al.'s (1998) results using the Ryzhenko model, and the dashed line is

calculated from Akinfiev and Zotov's (2001) HKF parameters. For Cu-HS complexes, the solid line is fitted from Mountain and Seward's (1999; 2003) results using the Ryzhenko model, and the dashed line is calculated from Akinfiev and Zotov's (2001) HKF parameters.

Figure 12. Comparison of mineral solubility and predominant aqueous Cu(I) species in the Cu(I)-Cl^--HS^--H_2O system as a function of activities of the chloride and bisulfide ions at 325 ˚C. The plots were generated using the Geochemist's Workbench (Bethke, 2008). Figure (a) is calculated from the published formation constants based on experimental studies (e.g., Brugger et al. 2007; Liu W et al. 2005; Mountain and Seward, 1999, 2003), while in Figure (b), the formation constants for aqueous Cu(I) species are from MD simulation results of this study (Table 2).

Figure 13. Aqueous copper species (a, b), total concentration of copper in aqueous fluid (c), and mineral assemblages (d) as a function of total sulfur concentration (existing mainly as HS^- in solution) at 325 ˚C and 500 bar. subplot a is based on properties from available experimental data (Brugger et al. 2007; Liu W et al. 2005; Mountain and Seward, 1999, 2003) and subplot b is based on MD. In subplot c and d, the red lines are based on properties from available experimental studies while the blue lines are based on MD (Table 2), see text for the composition of initial fluid and details of the modelling).

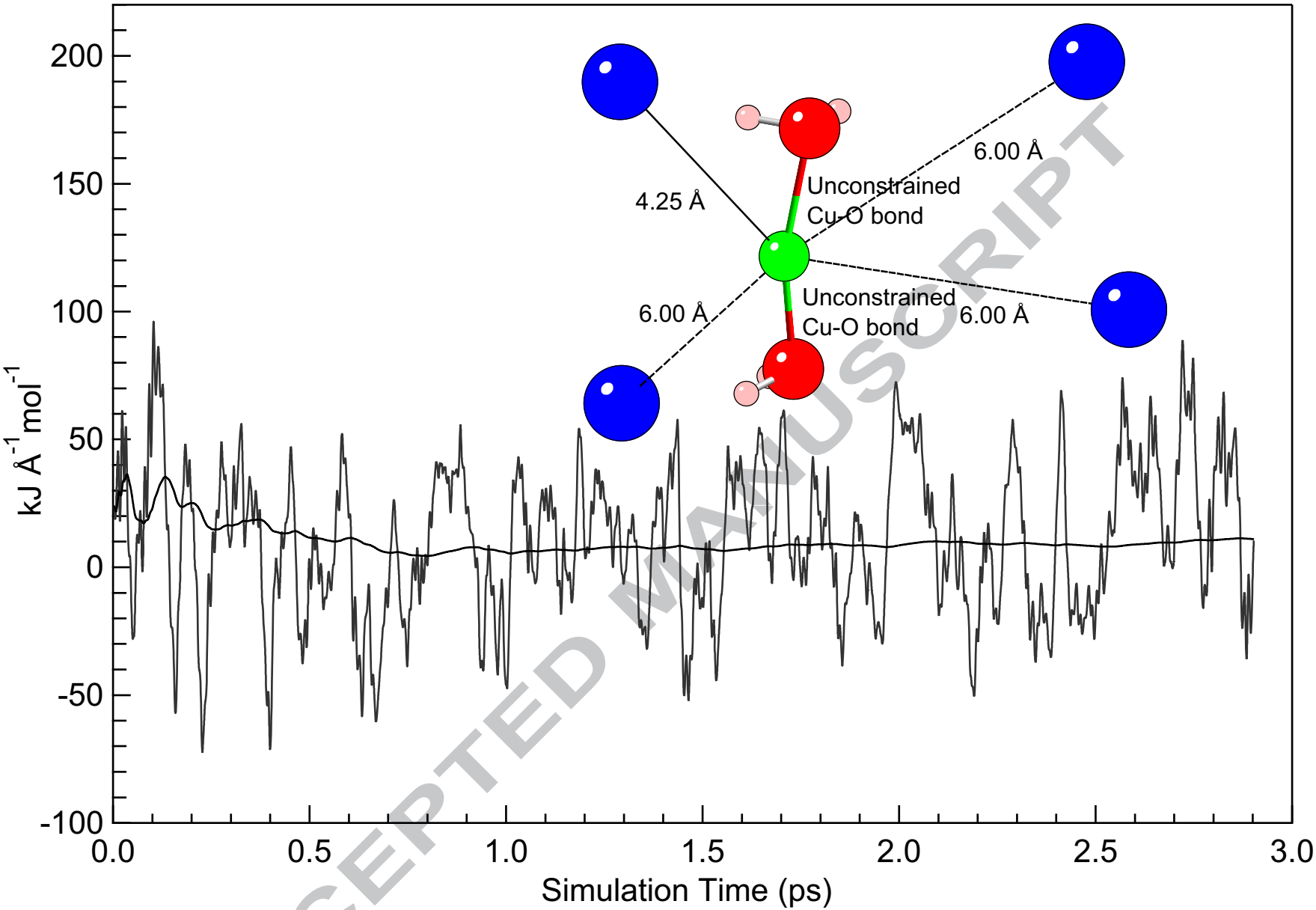

(a)

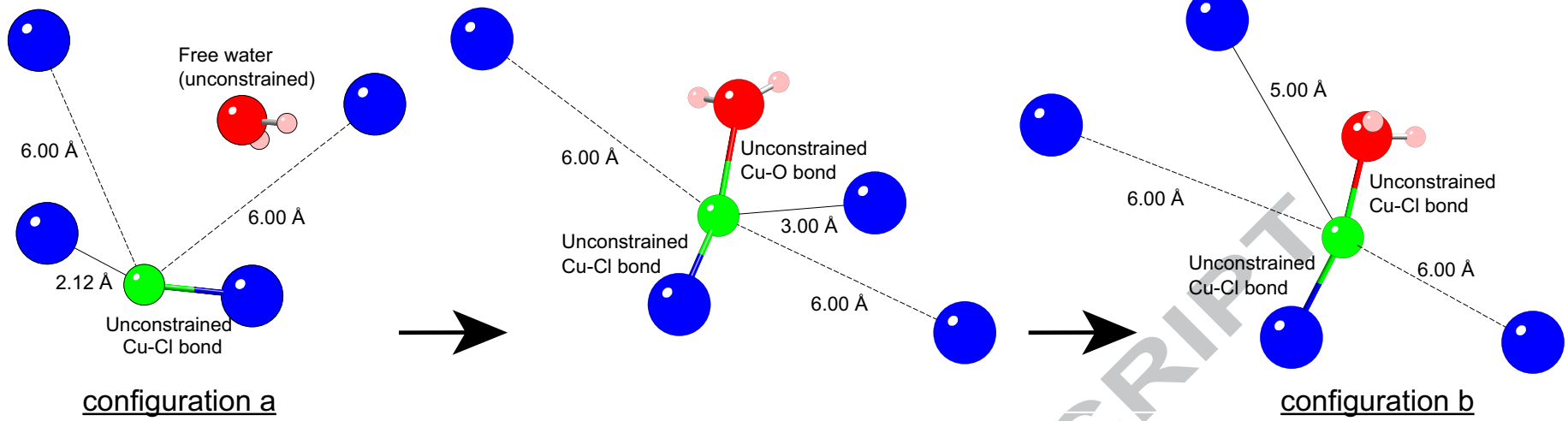

configuration a

configuration b

(b)

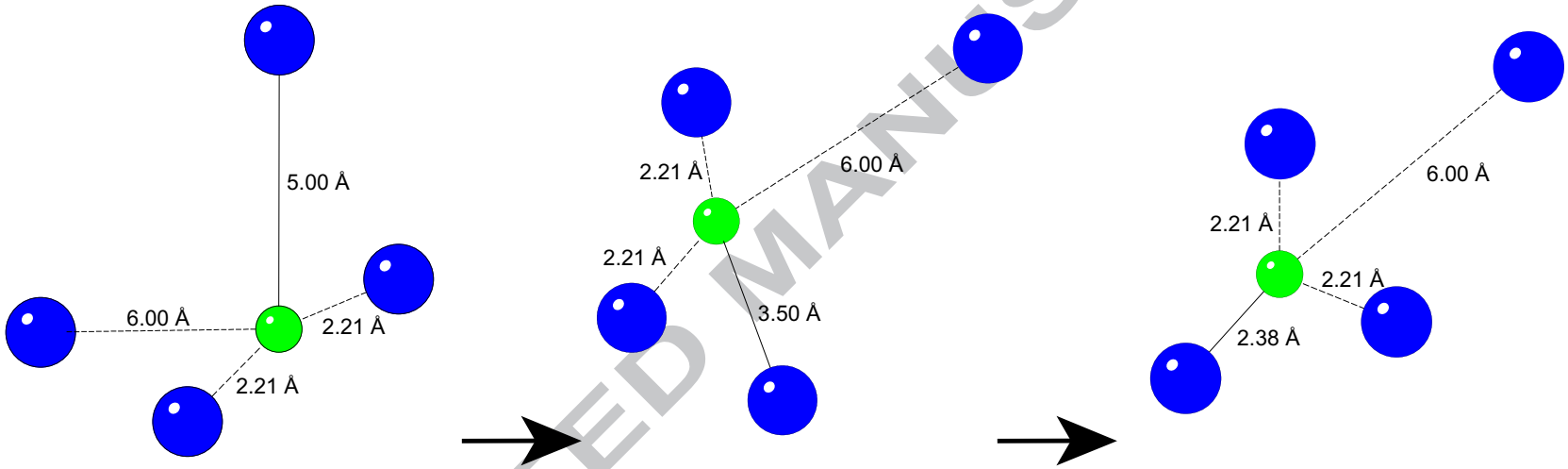

configuration a

configuration b

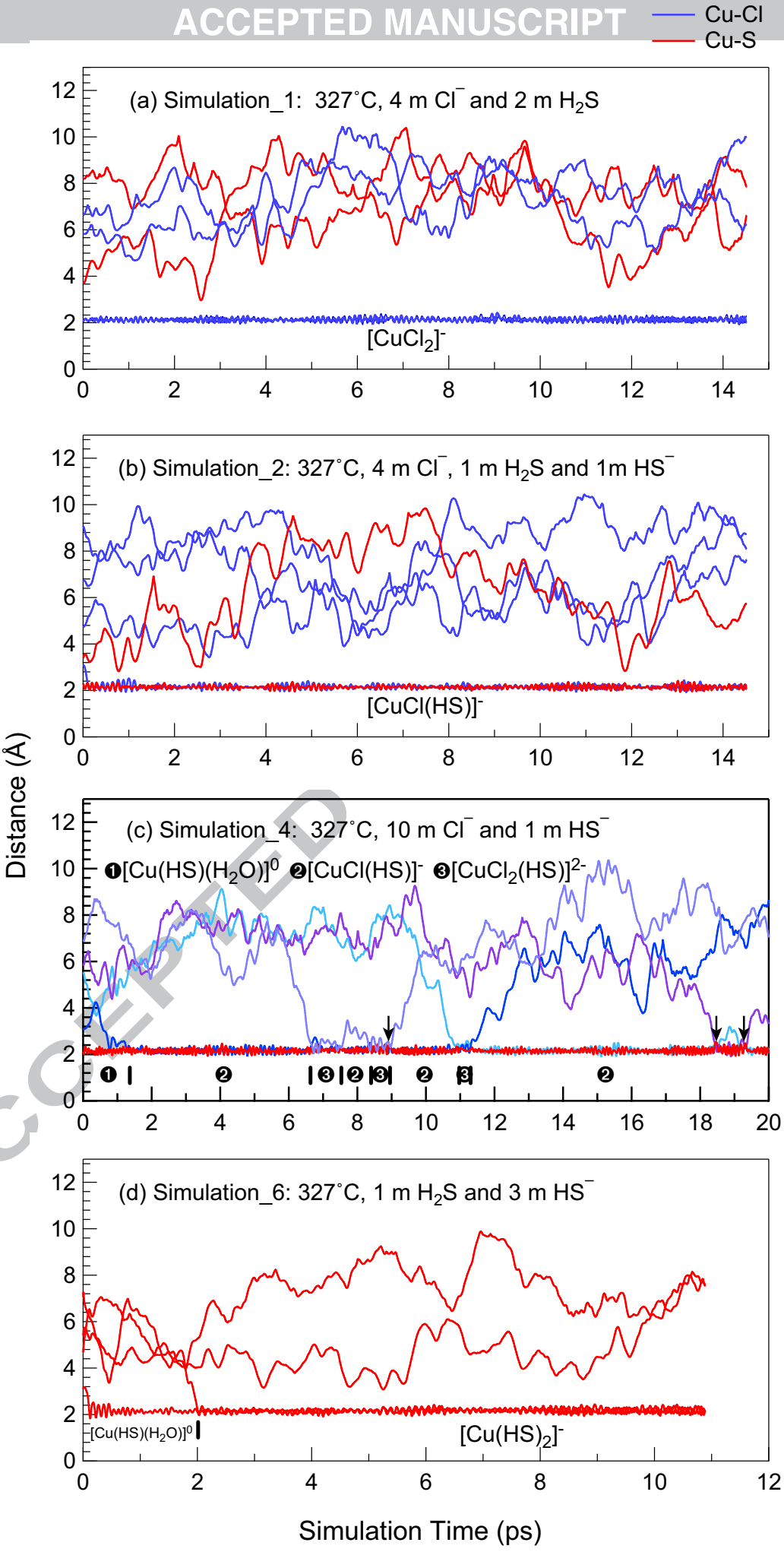

Figure 4

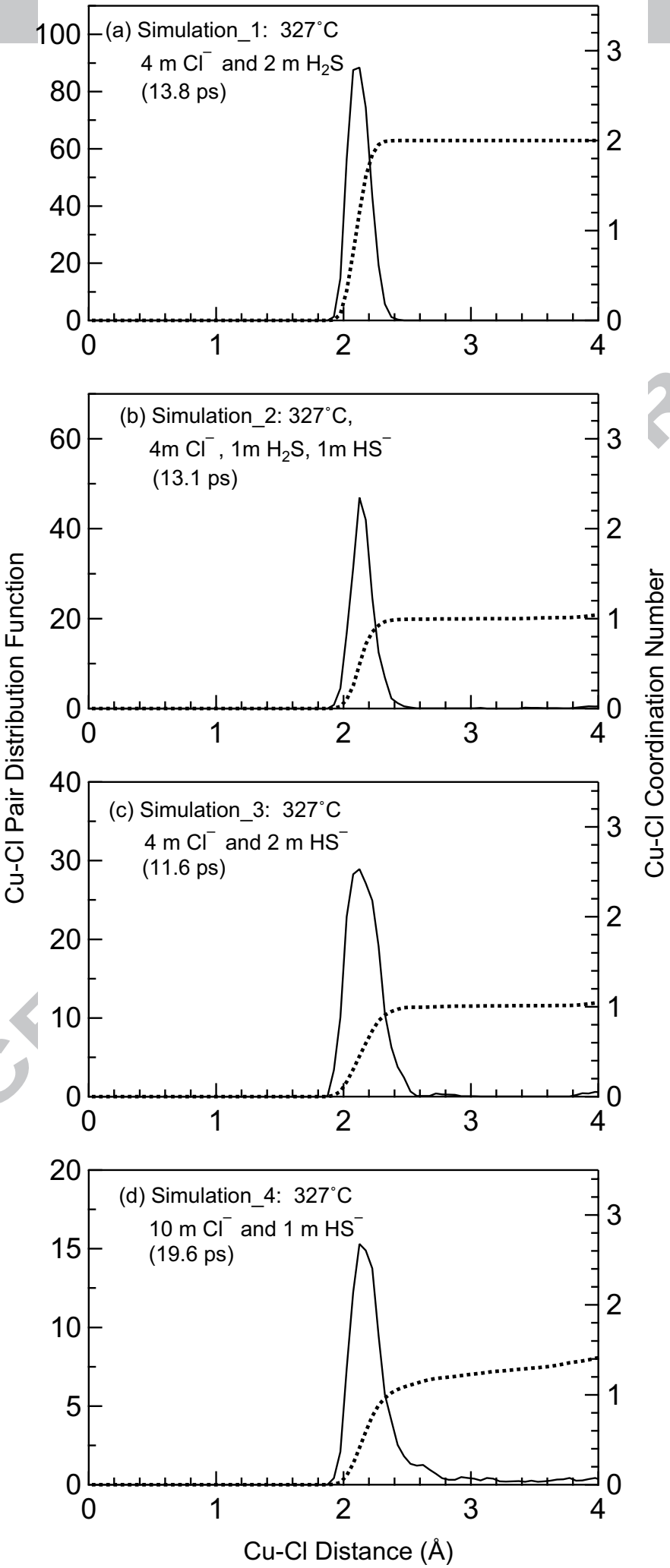
(a) Simulation_1: 327˚C
4 m Cl⁻ and 2 m H2S
(13.8 ps)
(b) Simulation_2: 327˚C,
4m Cl⁻ , 1m H2S, 1m HS⁻
(13.1 ps)
(c) Simulation_3: 327˚C
4 m Cl⁻ and 2 m HS⁻
(11.6 ps)
(d) Simulation_4: 327˚C
10 m Cl⁻ and 1 m HS⁻
(19.6 ps)
Cu-Cl Pair Distribution Function
Cu-Cl Coordination Number
Cu-Cl Distance (Å)

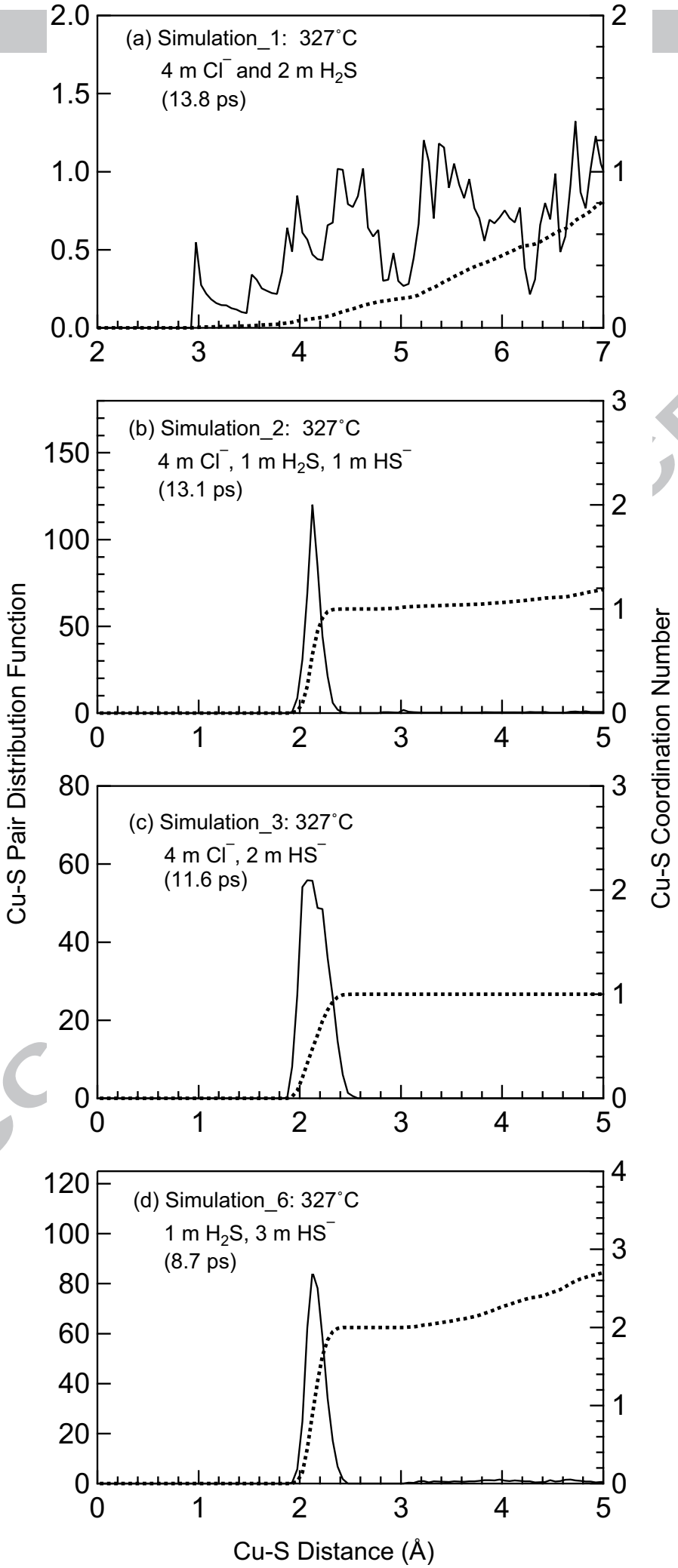
(a) Simulation_1: 327˚C
4 m Cl⁻ and 2 m H2S
(13.8 ps)
(b) Simulation_2: 327˚C
4 m Cl⁻, 1 m H2S, 1 m HS⁻
(13.1 ps)
(c) Simulation_3: 327˚C
4 m Cl⁻, 2 m HS⁻
(11.6 ps)
(d) Simulation_6: 327˚C
1 m H2S, 3 m HS⁻
(8.7 ps)
Cu-S Pair Distribution Function
Cu-S Coordination Number
Cu-S Distance (Å)

Figure 6

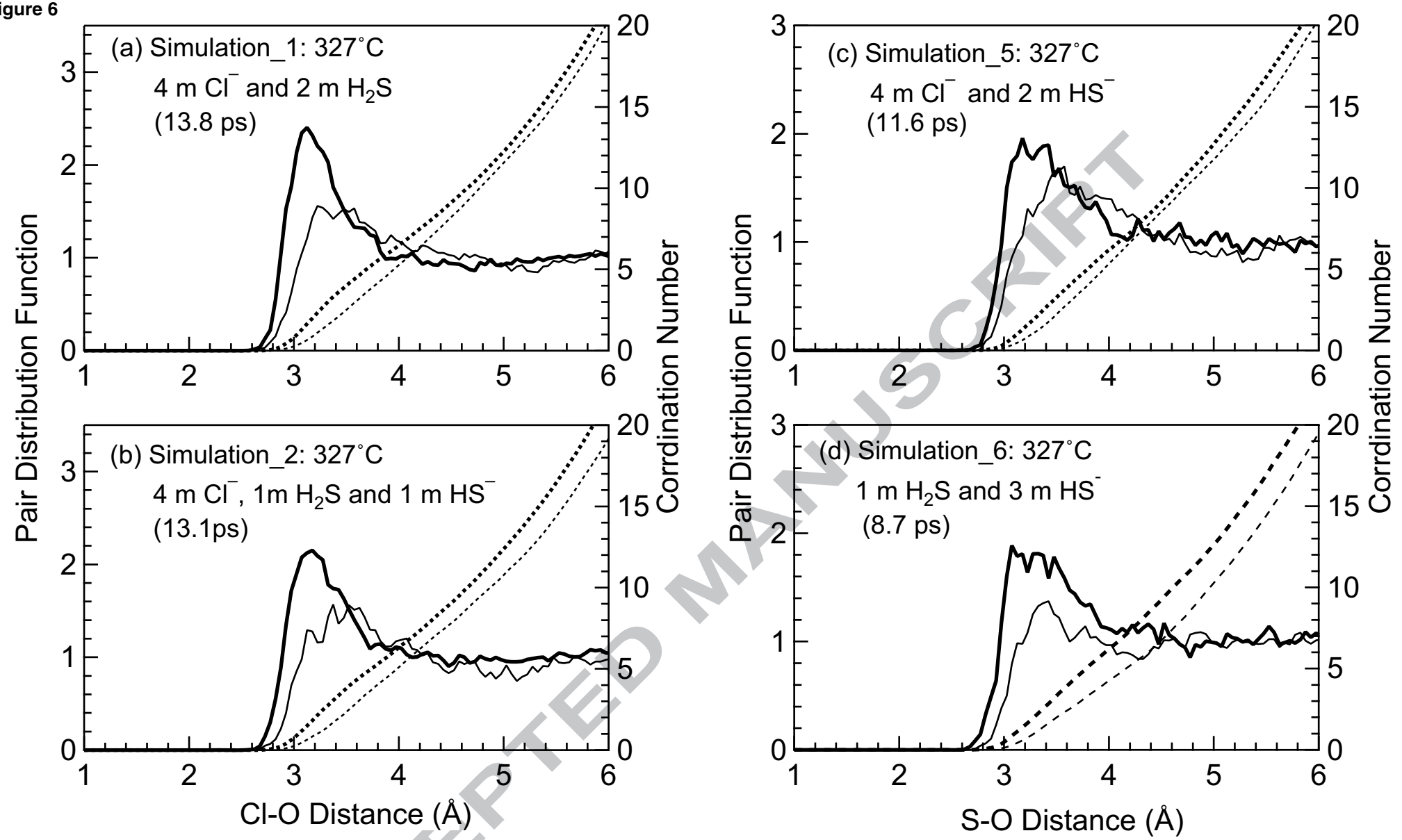

Figure 7

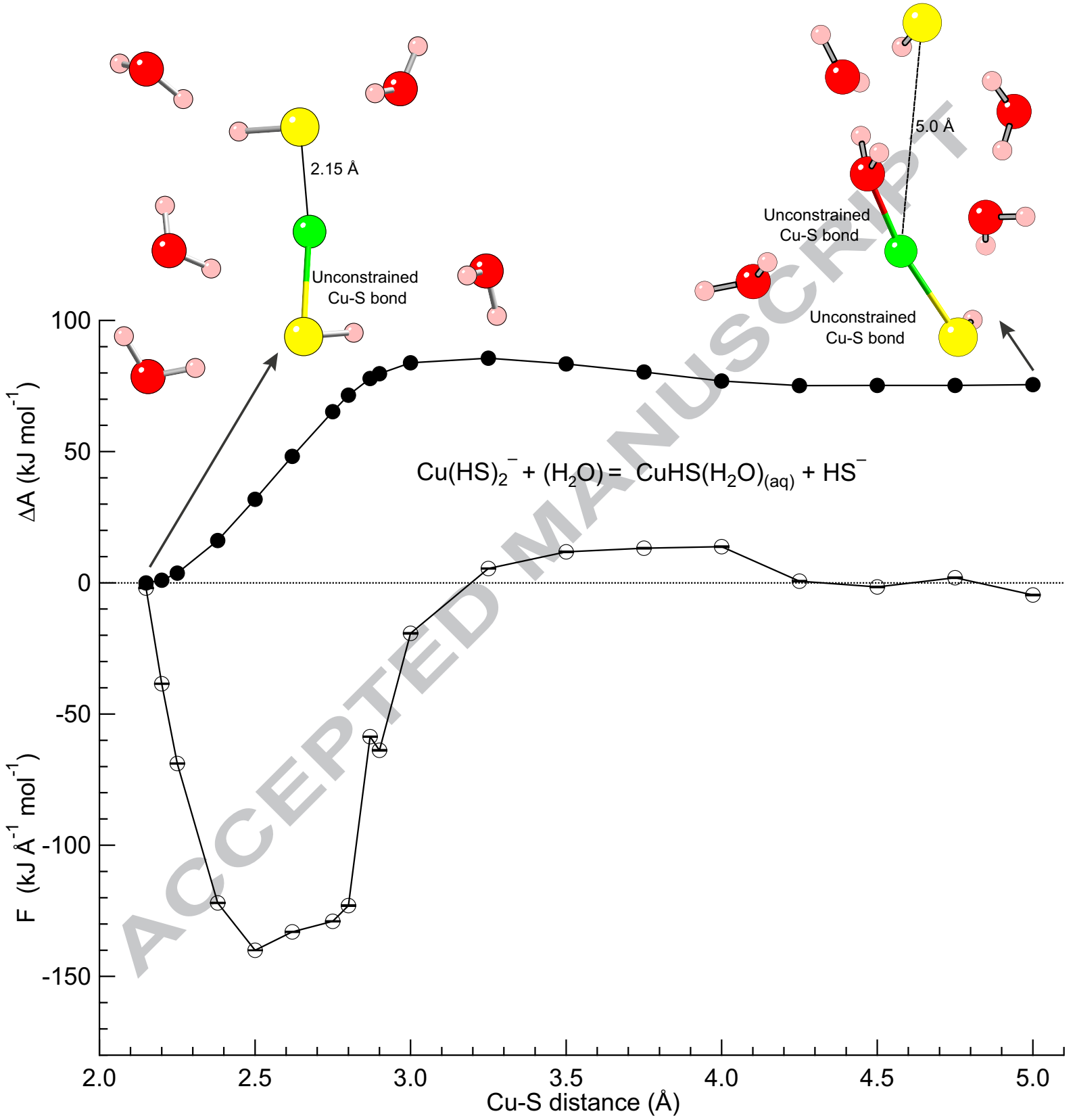

Figure 8

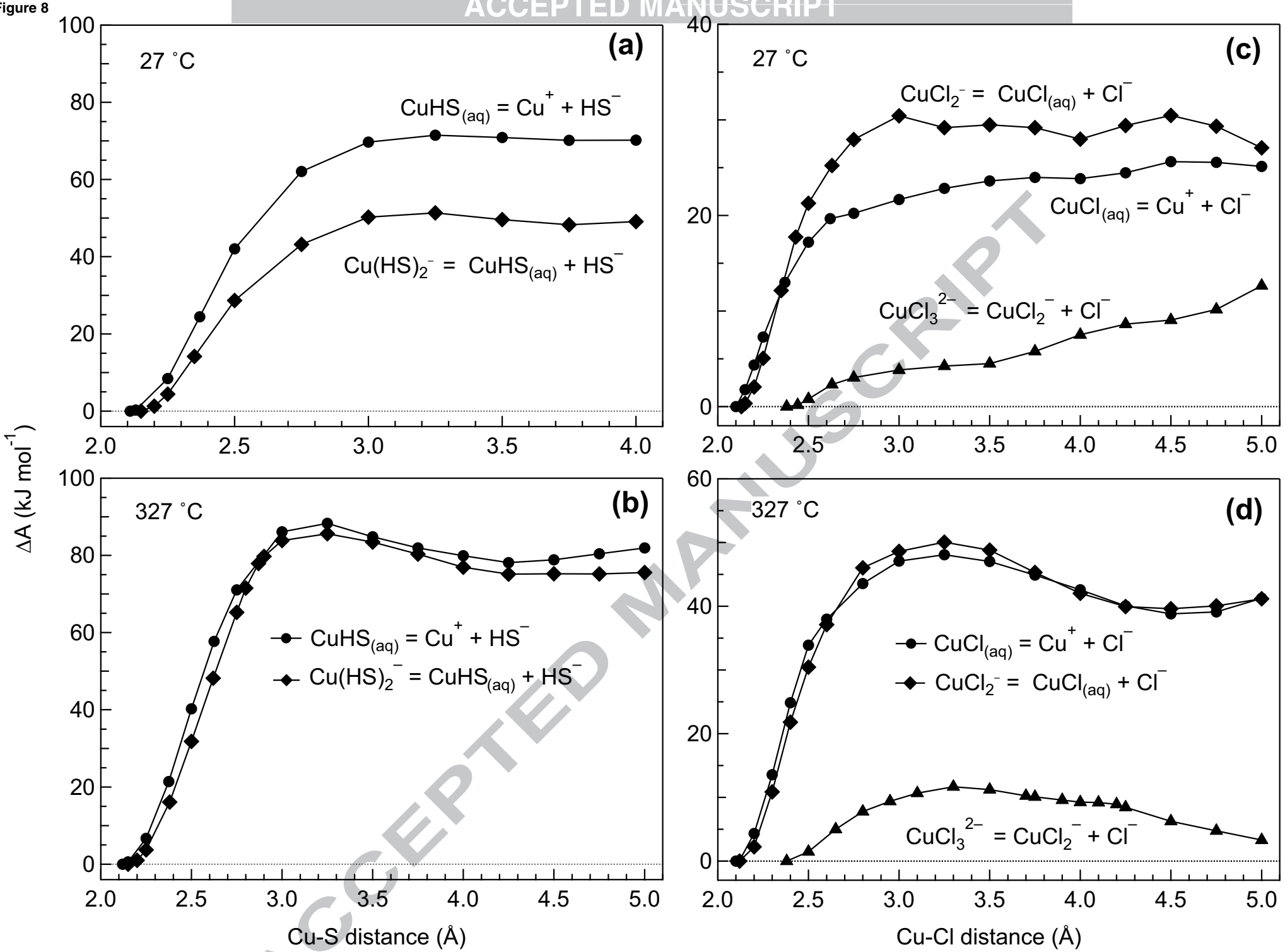

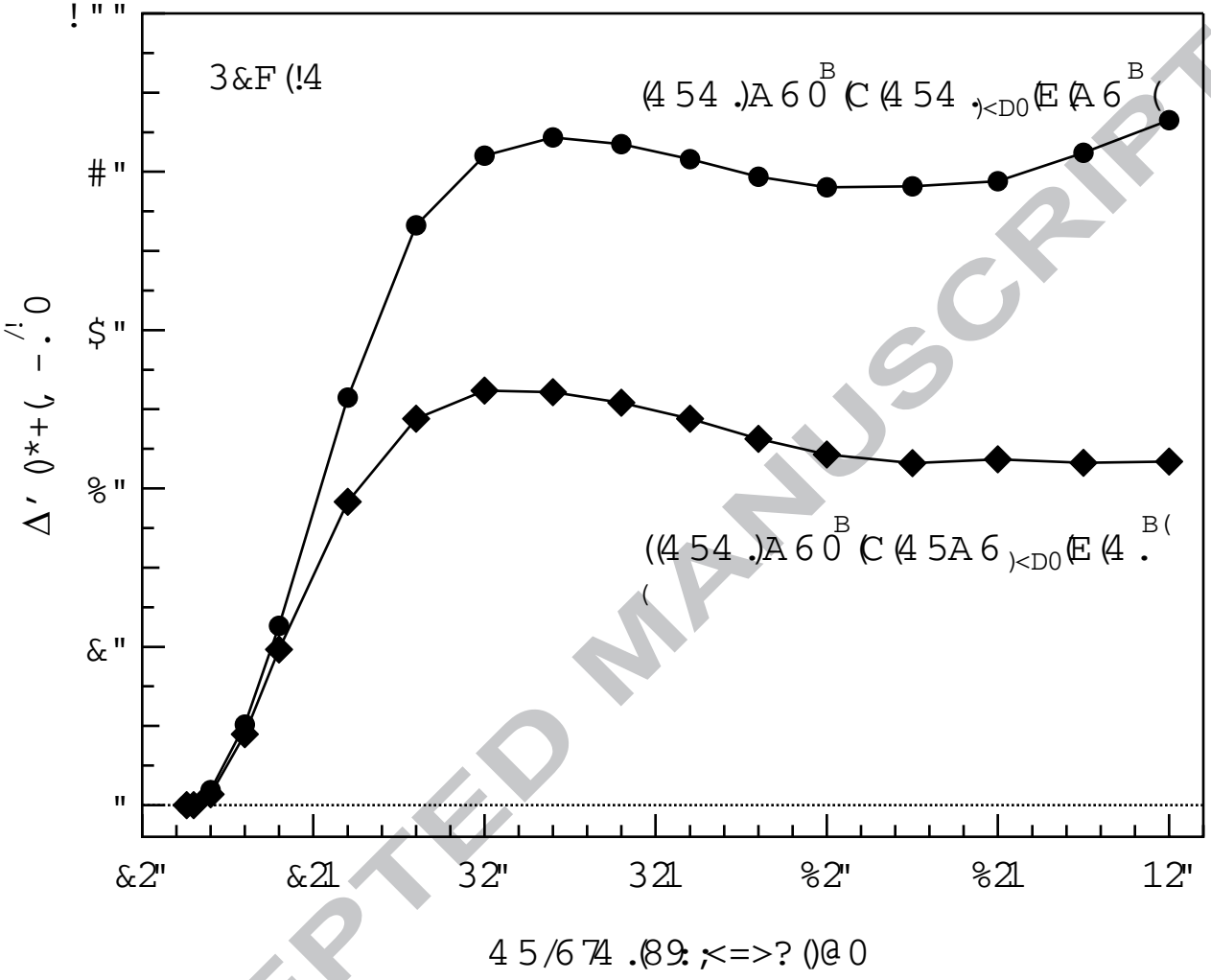

(a) $Cu(H_2O)_2^+$

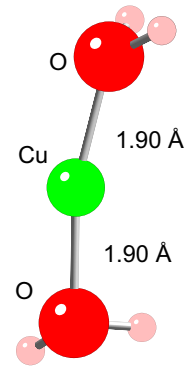

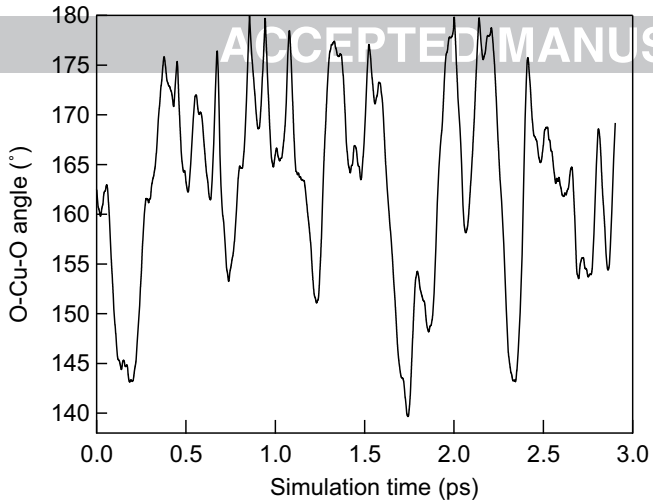

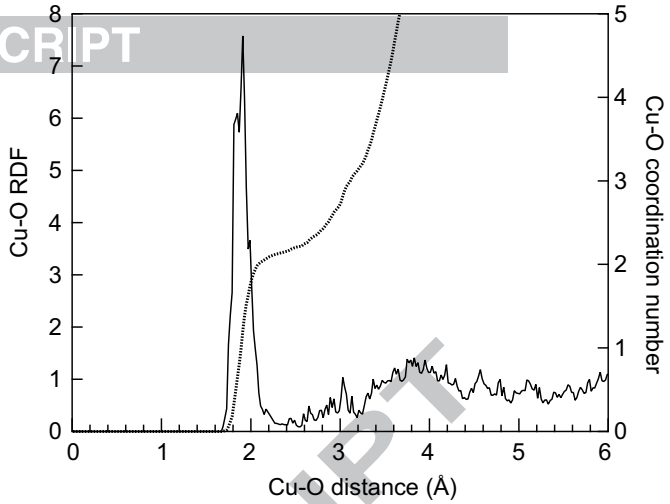

(b) $CuCl(H_2O)_{(aq)}$

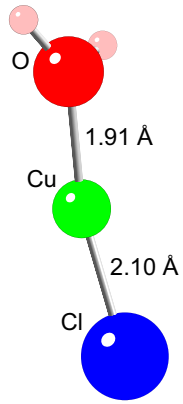

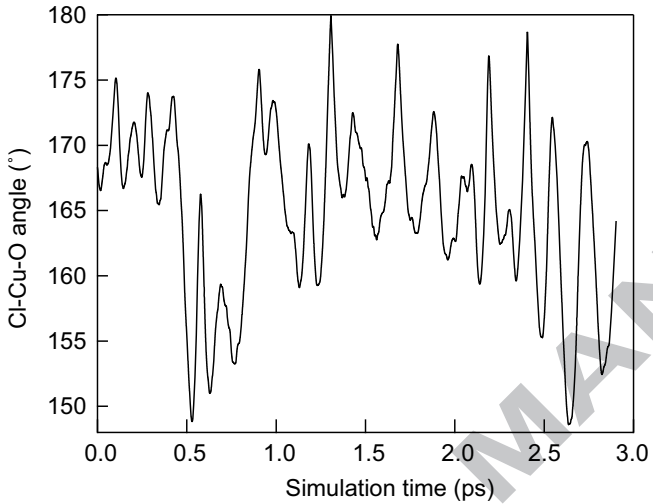

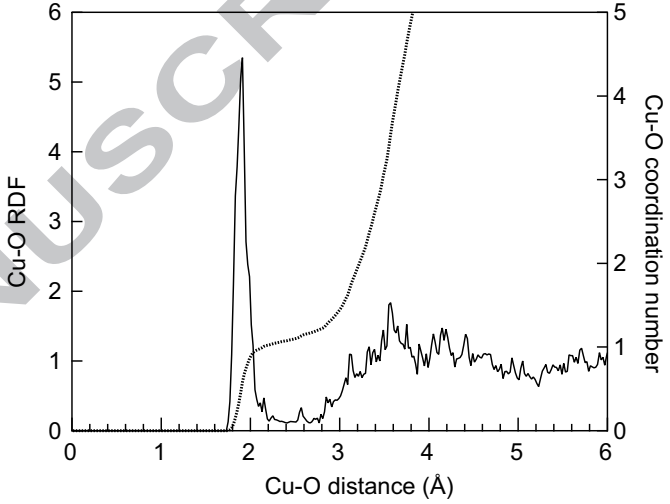

(c) $Cu(HS)(H_2O)_{(aq)}$